Received: 15 September 2017 | Revised: 17 January 2018 | Accepted: 21 February 2018

DOI: 10.1002/joc.5507

International Journal of Climatology RMetS

RESEARCH ARTICLE

Linking atmospheric circulation patterns with hydro-geomorphic disasters in Peru

C. Rodríguez-Morata[1] | J. A. Ballesteros-Canovas[1] | M. Rohrer[1,2] | J. C. Espinoza[3] | M. Beniston[1] | M. Stoffel[1,4,5]

[1]Climate Change Impacts and Risks in the Anthropocene (C-CIA), Institute for Environmental Sciences, University of Geneva, Geneva, Switzerland

[2]Meteodat GmbH, Zurich, Switzerland

[3]Instituto Geofísico del Perú (IGP), Subdirección de Ciencias de la Atmósfera e Hidrósfera (SCAH), Lima, Peru

[4]Dendrolab.ch, Department of Earth Sciences, University of Geneva, Geneva, Switzerland

[5]Department F.-A. Forel for Aquatic and Environmental Research, University of Geneva, Geneva, Switzerland

Correspondence

C. Rodríguez-Morata, Climatic Change and Climate Impacts, Institute for Environmental Sciences, University of Geneva, Boulevard Carl-Vogt 66, CH-1205 Geneva, Switzerland.
Email: clara.rodriguez@unige.ch

Funding information

Swiss Agency for Development and Cooperation

The occurrence of El Niño has been generally considered the main driver of hydro-geomorphic processes in Peru. However, the climatic characterization of hydro-geomorphic events (HGE) occurring in the absence of El Niño remains scarce. Information contained in the DesInventar disaster database suggests a widespread occurrence of HGE associated to cold-neutral sea surface temperature (SST) in the central Pacific and south tropical Atlantic. Here, we aim at characterizing synoptic patterns associated with HGE that have occurred over last 35 years related to the different El Niño types and focusing as well on the non-Niño phases. We use the ERA-Interim reanalysis climate data and implement self-organizing maps to assess the link between HGE in Peru and specific synoptic patterns. Results suggest that synoptic patterns associated with La Niña and neutral conditions play an important role in the occurrence of hydro-geomorphic disasters in Peru during the austral summer. A total of 21% of the events are associated only with the 1972–1973, 1982–1983 and 1997–1998 El Niño events and are mainly focused in the northern Pacific coast of the country (i.e., Tumbes, Piura and Lambayeque) while more than 36% of the recorded events in the database were associated with La Niña and neutral conditions between 1970 and 2013. La Niña-related events were more relevant in the Andean–Amazonian regions, whereas neutral conditions were related to more frequent HGEs in the southern regions (south of the 13.25°S) along the Peruvian Pacific coast. These outcomes imply an enhanced understanding of the synoptic mechanisms leading to the occurrence of HGE and contribute to a better understanding of the triggers of HGE causing disaster no exclusively related to El Niño-like years in Peru.

KEYWORDS

ENSO phases, hydro-geomorphic events, Peru, self-organizing maps, synoptic patterns

1 | INTRODUCTION

Hydro-geomorphic events (hereafter referred to as HGE and comprising floods, flash floods, landslides, and debris flows) repeatedly cause large economic losses and casualties in South America (Comunidad Andina, 2008; DesInventar, 2015). During the period 1970–2006, more than 12,000 HGE events have been recorded in Peru (Comunidad Andina, 2008). These events have claimed more than 7,600 lives and affected more than 244,000 properties, of which approximately 60,000 were destroyed completely. HGE are common in the flanks of the mountain ranges and valleys and they are related to steep slopes, lithology, heavy rainfall, earthquakes, and an inadequate land use (Margirier, Audin, Carcaillet, Schwartz, & Benavente, 2015; Morera, Condom, Crave, Steer, & Guyot, 2017; Vargas et al., 2010;

Villacorta, Fidel, & Zavala, 2012; Zavala & Núñez, 1999). Their origin is connected with the location of Peru in an active convergent boundary which determines the local geology and tectonic settings (Zavala & Núñez, 1999). They occur as a result of heavy rainfalls, which normally occur between December and April and during extreme hydro-climatic events, like El Niño–Southern Oscillation (ENSO) phenomena (Zavala, Rosado, & León, 2012). Recent examples of these events were those took place during the 2017 austral summer season in Peru, where more than 100 people died and nearly 1 million people were affected (Instituto Nacional de Defensa Civil, 2017).

The single-most important global climate feature, the ENSO, has been shown to play a key role in the triggering of rainfall-induced HGE disasters in Peru (Lavado-Casimiro, Felipe, Silvestre, & Bourrel, 2013; Rau et al., 2017; Takahashi, 2004; Waylen & Caviedes, 1986). ENSO results from the interaction between the tropical Pacific Ocean and atmosphere and is considered to represent the most dominant modes of inter-annual variability resulting in considerable variability in rainfall at the global scale (Brönnimann, 2007; Power, Casey, Folland, Colman, & Mehta, 1999; Power, Delage, Chung, Kociuba, & Keay, 2013; Ropelewski & Halpert, 2007). ENSO is related to sea surface temperature (SST) variability in the equatorial Pacific Ocean which is accompanied by larger-scale fluctuations in air pressure known as the Southern Oscillation. This is an east–west see-saw-like movement of air masses between the Pacific and the Indo-Australian areas (World Meteorological Organization, 2014). The hydrological impacts over Peru are complex: while warm conditions over the East Pacific (i.e., eastern El Niño or coastal El Niño) produce abundant rainfall over the Peruvian coast, warm conditions over the central equatorial Pacific (i.e., central El Niño) produces lack of precipitation over the Andes and the Amazon basin (Espinoza et al., 2011; Lagos, Silva, Nickl, & Mosquera, 2008; Lavado-Casimiro & Espinoza, 2014; Sulca, Takahashi, Espinoza, Vuille, & Lavado-Casimiro, 2017). In addition, floods in the Peruvian Amazonas have been attributed to cold conditions over the central equatorial Pacific (Espinoza, Lengaigne, Ronchail, & Anicot, 2012; Espinoza, Ronchail, Frappart, et al., 2013; Marengo et al., 2013; Marengo & Espinoza, 2016).

Specifically in Peru, major impacts were recorded during the El Niño events in 1982–1983 and 1997–1998 (Cai et al., 2014; Dewitte et al., 2014; Frey et al., 2016; Magilligan & Goldstein, 2001; McPhaden, 1999; Rocha, 2007), during the 1925 El Niño (Takahashi & Martínez, 2017), and recently during the austral summer of 2015–2016 (CPC/IRI, 2016; L'Heureux et al., 2017). Disasters observed during the 1997–1998 El Niño episode evidenced the need for early, long-term (i.e., seasonal) forecasts in Peru (Bayer et al., 2014) as well as the definition of national civil protection laws. Since this late 20th century disaster, the Peruvian government is legally bound to develop disaster management plans centred on the preservation of infrastructure, the management of proper drainage channels for excess rainwater, and the distribution of emergency aid to the population (Glantz, 2001). As a consequence, much research effort has been invested into the analysis and description of the mechanisms involved in the inception of El Niño (Liu et al., 2014; Su, Li, & Zhang, 2014; Yu, Kao, & Lee, 2010), different El Niño types (Ashok, Behera, Rao, Weng, & Yamagata, 2007; Kug, Jin, & An, 2009; Takahashi, Montecinos, Goubanova, & Dewitte, 2011), and the temporal evolution of El Niño phenomena (Moy, Seltzer, Rodbell, & Anderson, 2002; Rein et al., 2005; Wittenberg, 2009). At the same time, however, an increasingly large core of historical evidence and recent events points to the crucial role of HGE disasters occurring during austral summers in the absence of El Niño phenomena (DesInventar, 2015; Villacorta, De Torres, Pérez-Puig, Llorente, & Ayala, 2015), which can be related to low-frequency modes of variability in SST and rainfall over the Andes (e.g., Neukom et al., 2015; Segura, Espinoza, Junquas, & Takahashi, 2016). Yet, there has been little systematic analysis of the synoptic situations leading to HGE disasters in Peru during La Niña and neutral conditions and this topic has received substantially less attention compared to those events triggered by El Niño phenomena. Nowadays, the situation is even such that this lack of attention to La Niña and neutral conditions has become an obstacle for a more appropriate awareness of hazards among local populations and authorities.

Climate synoptic patterns have traditionally been analysed with principal component analysis (PCA) as well as with empirical orthogonal functions (EOF), terms which are often used interchangeably in the literature (Cohen, 1983; Kutzbach, 1967; Lorenz, 1965; Smith, Reynolds, Livezey, & Stokes, 1996; Walsh, 1978). Other approaches have included rotated EOFs (Barnston & Livezey, 1987), *k*-means cluster analyses (Michelangeli, Vautard, & Legras, 1995), and/or empirical orthogonal teleconnections (Van den Dool, Saha, & Johansson, 2000). All of the above approaches assume that the continuum atmospheric states may be split into a limited number of categories with clear boundaries. The PCA approach thereby generates a set of mathematically orthogonal (uncorrelated) variables that, from a statistical perspective, will represent variance in a data set most adequately (Jolliffe, 2002). Besides, several studies (Buell, 1975; Jolliffe, 2002; Preisendorfer & Mobley, 1988; Richman, 1986; Von Storch & Zwiers, 1999) have broadly reported shortcomings and limitations of PCA, especially when it comes to the analysis of data with nonlinear characteristics. In fact, the nonlinearities of climate data are cancelled by the use of linear measures (e.g., correlation), the enforced orthogonality (Hurrell, Kushnir, Ottersen, & Visbeck, 2003), and the non-inherently physical meaning of the components since each component is a statistical representation of the variance of the data set (Barry & Carleton, 2001; Peixoto & Oort, 1992).

These potential limitations can be overcome by using self-organizing maps (SOM) (Hewitson & Crane, 2002; Kohonen, 2001) since the approach differs from linear analysis by providing additional skills for nonlinear data sets (Reusch, Alley, & Hewitson, 2005). This neural network approach therefore provides a technique to summarize large, high-dimensional records by treating data as a continuum rather than as discrete classes. SOM also identify patterns through the use of an iterative clustering algorithm (Hewitson & Crane, 2002) and thereby produce a set of nodes (i.e., generic synoptic states directly interpretable as physical process states) in a two-dimensional lattice with similar states close to each other and the most extreme states at the opposite corners. Consequently, SOM analyses easily allow characterization of time trends in the frequency of occurrence and transitions of selected patterns (Kohonen, 2001; Hewitson & Crane, 2002). This technique has been successful for many meteorological, climatological, and oceanic research initiatives worldwide, either to characterize extreme weather and rainfall events (Cassano, Lynch, Cassano, & Koslow, 2006; Cassano, Uotila, & Lynch, 2006; Hong, Hsu, Sorooshian, & Gao, 2005; Morata, Martin, Luna, & Valero, 2006; Schuenemann, Cassano, & Finnis, 2009; Uotila, Lynch, Cassano, & Cullather, 2007; Zhang, Wang, Liu, Ahu, & Wang, 2006), including in Peruvian Amazon and Andes (Espinoza et al., 2012; Espinoza, Ronchail, Lengaigne, et al., 2013; Paccini, Espinoza, Ronchail, & Segura, 2018), to visualize synoptic weather patterns over a region (Hewitson & Crane, 2002; Johnson, Feldstein, & Tremblay, 2008; Reusch, Alley, et al., 2005; Reusch, Alley, & Hewitson, 2007; Reusch, Hewitson, & Alley, 2005; Seefeldt & Cassano, 2008; Wise & Dannenberg, 2014), or to evaluate global climate model (GCM) results (Cassano, Uotilla, Lynch, & Cassano, 2007; Lynch, Uotila, & Cassano, 2006; Skific, Francis, & Cassano, 2009a, 2009b).

In this article, we aim at (a) analysing spatio-temporal patterns of HGE disasters in Peru; (b) determining their occurrence under El Niño, La Niña, and neutral conditions; and (c) assessing the frequency of occurrence of these patterns over time. We use a large data set of HGE disasters covering the last three decades from existing, systematic records and reanalysis data from the European Centre for Medium-Range Weather Forecasts (ECMWF). We interpret the occurrence of HGE disasters with SOM so as to identify synoptic patterns leading to the occurrence of HGE events.

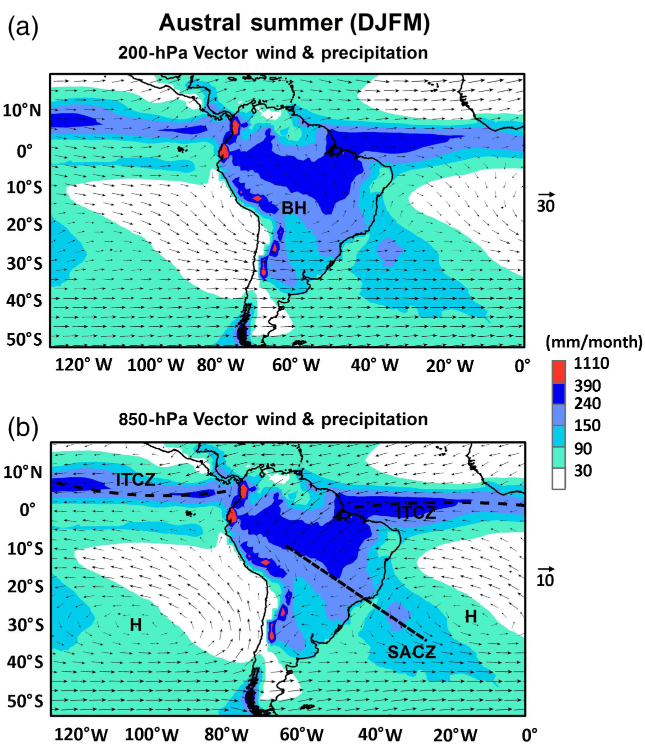

FIGURE 1 South American austral summer (DJF) climatology showing 1981–2010 ERA-Interim total precipitation means associated with the South American monsoon: (a) 200 hPa wind vectors U/V and position of the BH; (b) 850 hPa wind vectors U/V and position of the main climatic features present during the austral summer (H = high-pressure centres over the Pacific (left) and Atlantic (right) oceans) [Colour figure can be viewed at wileyonlinelibrary.com]

2 | ATMOSPHERIC CIRCULATION AND HYDRO-CLIMATIC VARIABILITY DURING THE PERUVIAN AUSTRAL SUMMER

During the austral summer (DJFM), atmospheric circulation over the area is dominated by the mature phase of the South American monsoon system (Vera et al., 2006; Zhou & Lau, 1998) and the reinforcement of deep convection over the south central Amazon basin (Garreaud, Vuille, Compagnucci, & Marengo, 2009; Marengo, Lieberman, et al., 2012; Vera et al., 2006). The southeast development of monsoon precipitation from the Amazon basin towards the western South Atlantic forms a band of convective activity and high precipitation known as the South Atlantic convergence zone (SACZ) (Figure 1b). The maximum intensity of the SACZ is centred on the austral summer (Barreiro, Chang, & Saravanan, 2002; Carvalho, Jones, & Liebmann, 2004; Figueroa, Satyamurty, & Da Silva Dias, 1995; Kodama, 1992), when it is coupled with the convection over the south central part of the continent, resulting in heavy rainfall episodes over southeastern South America (Liebmann, Kiladis, Marengo, Ambrizzi, & Gilck, 1999).

At low tropospheric levels (Figure 1b), the SACZ is characterized by the convergence of warm and moist air, which comes from the west (i.e., strong northwesterly flow along the Andes between 10°S and 20°S) and from the north (i.e., a westwards extension of the South Atlantic High [SAH]). The SACZ is, moreover, linked to the tropical easterlies and bringing flows into the continent at about 15°S latitude (Lenters & Cook, 1995). At high levels (i.e., 200 hPa), the Bolivian High (BH) (Figure 1a) is the major synoptic feature occurring during austral summers (Lenters & Cook, 1997). It consists in a closed anticyclone developing over the central Andes, which forms in response to latent heat released during deep convection over the Amazon basin (Sulca, Vuille, Silva, & Takahashi, 2016). The BH is connected over the central Andes with mid- and upper-level easterly winds and facilities the transport of moist air coming from the Amazon basin and the Atlantic Ocean onto the central Andes. This moist air influx feeds convective storms responsible of almost the 80% of the annual precipitation total (350–400 mm) in the central Andes during the austral summer (DJFM) (Falvey & Garreaud, 2005; Garreaud, 1999, 2000; Garreaud, Vuille, & Clement, 2003; Sulca et al., 2016; Vuille, 1999; Vuille, Bradley, & Keimig, 2000; Vuille & Keimig, 2004).

Three major types of circulation anomalies exist in the region, operating at intra-seasonal timescales, namely, extra-tropical cyclones, cold-core lows, and the westwards amplification of the SAH (Lenters & Cook, 1999). These anomalies are associated with rainy periods on the Altiplano, supported by the moist-polewards flow at low levels along the eastern flank of the central Andes, which also largely explains the high rainfall rates occurring during this situation (e.g., Espinoza, Segura, Ronchail, Drapeau, & Gutierrez-Cori, 2016; Paccini et al., 2018). In addition, the warm, low-level flow along the SACZ deepens the overlying atmospheric column, thereby resulting in an intensification and southwards shift of the BH (Lenters & Cook, 1999), which in turn results in wetter days on the Altiplano. Consequently, the position of the SACZ plays a crucial role in the variability of both the BH and rainfall on the Altiplano. The strength and position of the BH are controlled, moreover, by the latent heat release during convection in the Amazon basin, which shapes the primary structure of the BH (Silva Dias, Schubert, & De Maria, 1983), and by the rainfall over the central Andes, which results in an enlargement and a southwards displacement of the BH (Lenters & Cook, 1997). Besides, convective activity over the SACZ and the BH is also modulated by other climate features. For example, extratropical Rossby waves propagating towards the Equator along the eastern coast of South America can influence the intensity and location of the SACZ (e.g., Carvalho et al., 2004; De Souza & Ambrizzi, 2006; Diaz & Aceituno, 2003; Kodama, Sagawa, Ishida, & Yoshikane, 2012; Kousky, 1979; Muza, Carvalho, Jones, & Liebmann, 2009). Alvarez, Vera, Kiladi, and Liebmann (2016) reported that the location and strength of the BH can also be modulated by intra-seasonal phenomena, such as the Madden–Julian oscillation (MJO) (Madden & Julian, 1994). The Altiplano region and the southern Peruvian Andes are mostly influenced by easterly winds at the upper troposphere (300–200 hPa), which modulate rainfall variability at several timescales going from diurnal cycles (Garreaud, 1999; Junquas et al., 2017), through inter-annual variability (Garreaud et al., 2003; Vuille, Bradley, Werner, & Keimig, 2003) to decadal–inter-decadal variability (Segura et al., 2016).

On the other hand, several studies have documented that hydro-climatic variability over the Andes and Amazon regions are also related to changes in Atlantic SST. Thus, warm conditions over the northern tropical Atlantic are associated with droughts in the Peruvian Amazon (Espinoza et al., 2011, 2016; Espinoza Villar et al., 2009; Fernandes et al., 2011; Yoon & Zeng, 2010) and over the Peruvian Andes (Lavado-Casimiro et al., 2013; Lavado Casimiro, Ronchail, Labat, Espinoza, & Guyot, 2012). Besides, warm conditions over the tropical South Atlantic have been also associated with floods in the northern Peruvian Amazon (Marengo & Espinoza, 2016; Marengo, Tomasella, Soares, Alves, & Nobre, 2012). Over other regions like Cuzco, Puno, and Madre de Dios, extreme rainy events also appear during warm conditions of subtropical South Atlantic Ocean (Cavalcanti, Marengo, Alves, & Costa, 2016; Espinoza et al., 2014).

3 | MATERIAL AND METHODS

3.1 | Disaster database

We used the DesInventar database (DesInventar, 2015) to obtain information on the timing and the impact of climate-related disasters in Peru (Cutter et al., 2008; Cutter & Finch, 2008; Wisner, Blaikie, Cannon, & Davis, 2004). This data collection is the result of a cooperative work of researchers, academics, and institutions grouped in a network dedicated to social studies on disaster prevention in Latin America (or Red de Estudios Sociales en Prevención de Desastres en América Latina; LA RED, 1992). This initiative aims at overcoming the lack of disaster-related information in Latin America and at developing a system of data acquisition, gathering, and consulting so as to assess the typology and magnitude of past disasters. DesInventar collects information from pre-existing sources of information such as newspapers, official archives, and other historical records from a total of nine Latin American countries. For the period 1970–2013, the DesInventar entries available for Peru contain mainly newspaper articles published in *El Comercio* (the main Peruvian newspaper), but also documentary sources stored at the National Institute of Civil Defense (Instituto Nacional de Defensa Civil, 2010).

3.2 | Climate data and indices

Considering that impacts of El Niño/La Niña are contrasted over Peru if the event occurs over eastern or central equatorial Pacific (Lavado-Casimiro & Espinoza, 2014; Sulca et al., 2017), we used the *E* and *C* indices, introduced by Takahashi et al. (2011), to define El Niño and La Niña modes, based on the leading EOFs that account for extreme warm events in the eastern (*E* index) and cold/moderate warm events in the central equatorial Pacific (*C* index). After standardizing these indices, we define warmer-than-normal values as *E* and *C* values >0.5, and colder-than-normal values as *E* and *C* values <−0.5. In this sense, strong El Niño events are defined on the basis of values related with the 1982–1983 and 1997–1998 events (i.e., $C > 0.5$ and $E > 1$). Coastal El Niño events are associated with $E > 1$ and La Niña is defined based on *C* values ($C < -1$) as suggested by Lavado-Casimiro and Espinoza (2014). We also use the standardized SST gradient based on the difference between the north and south tropical Atlantic (NAT-SAT) (Enfield, Mestas-Nuñez, Mayer, & Cid-Serrano, 1999) as it influences the Peruvian rainfalls (Espinoza et al., 2011; Espinoza Villar et al., 2009; Lavado Casimiro et al., 2012). Neutral conditions are restricted to moments in which *E*, *C*, and NAT-SAT values range between −0.5 and 0.5.

The daily climatic analysis is based on the ERA-Interim reanalysis climate data set (European Centre for Medium-Range Weather Forecasts, 2016). ERA-Interim covers the period 1979 to present (Dee et al., 2011). Compared with its previous version ERA-40, this reanalysis not only improves the hydrological cycle as well as the quality of stratospheric circulation, but also handles biases and changes in the observing system in a more robust way (1957–2002) (Berrisford et al., 2009; Dee et al., 2011; Uppala et al., 2005). All climatic data used in this study were retrieved from http://www.ecmwf.int/research/era.

The domain of synoptic pattern analyses was delimited to latitudes ranging from 20°N to 60°S as well as to longitudes comprised between 140°W and 10°E (Figure 1). This area covers the entire South American continent and part of the East Pacific and West Atlantic oceans and is large enough to capture the main synoptic South American summertime features (i.e., the BH, the South American monsoon, SAH, intertropical convergence zone [ITCZ], and the SACZ), which are all strongly related to austral summer precipitation. For each grid point in the data set, we considered anomalies of geopotential (*Z*) and specific humidity (*Q*) at 200 and 850 hPa and by using a grid resolution of 2.5°. Analyses were performed at daily time steps for the period with higher HGE occurrence (i.e., December–April) during the period 1979–2013 (in total 5,143 days).

3.3 | Spatio-temporal analysis of HGE events

The domain of the spatio-temporal analysis of HGE disasters analysed here covers (a) the Pacific slopes of the Peruvian mountain ranges (we discern here between the northern [PN: Tumbes, Piura, and Lambayeque], central [PC: Libertad, Ancash, and Lima], and southern [PS: Ica, Arequipa, Moquegua, Tacna, Huancavelica, and Ayacucho] Peruvian mountain ranges) and (b) the Andean–Amazonian slopes

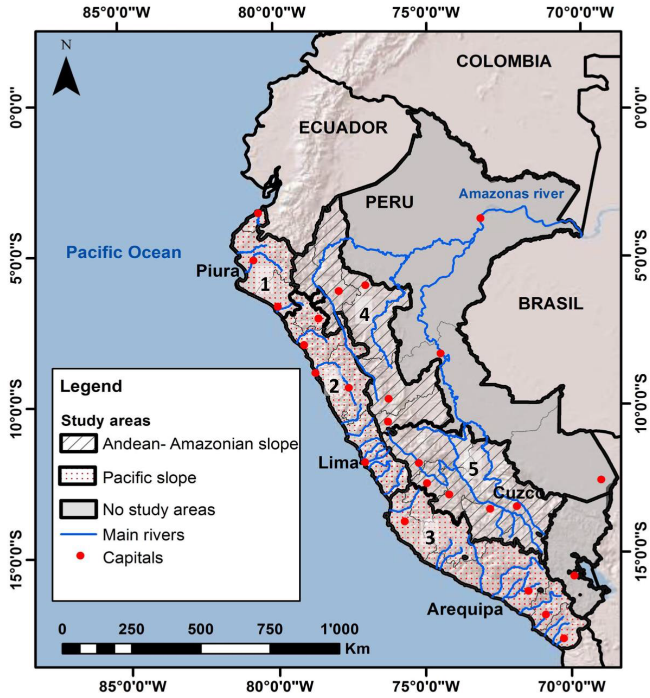

FIGURE 2 The study area is centred over two domains formed by Peruvian regions located (a) along the Pacific slopes (1 [north]: Tumbes, Piura, and Lambayeque; 2 [centre]: Libertad, Ancash, and Lima; 3 [south]: Ica, Arequipa, Moquegua, Tacna, Huancavelica, and Ayacucho) and (b) along the Andean–Amazonian slopes (4 [north]: Amazonas, Cajamarca, san Martin, Huánuco, and Pasco; 5 [south]: Apurimac, Cusco, Huancavelica, and Junin). Note that these domains are coincident with the two main river systems of Peru: Rivers running from east to west flow into the Pacific Ocean and rivers running from south to north flow into the Amazonas River [Colour figure can be viewed at wileyonlinelibrary.com]

(north [AN: Amazonas, Cajamarca, San Martin, Huánuco, and Pasco] and south [AS: Apurimac, Cusco, Huancavelica, and Junín] slopes) (Figure 2). This selection reflects the areas with the largest population densities and HGE impact and takes account of rainfall variability related to El Niño or La Niña events (Lavado-Casimiro & Espinoza, 2014). The spatio-temporal analysis of HGE started with a homogenization of the data set so as to capture all rain-induced events, including "generic rainfall-related damage" (i.e., muddy areas, structural damage, holes, etc.). We therefore discarded events induced by seismic activity, gravitational landslides, and anthropogenic floods such as the failure of pipes, dams, and other types of infrastructure. The information contained in the database was then included in ArcGIS to perform the spatial analyses of HGE occurrences between 1970 and 2013 to assess dissimilar occurrences of HGE at each region. Since DesInventar provides the exact date of disaster occurrences, the seasonality and the timing of HGE events was surveyed as well. Furthermore, an inspection of any relationship between ENSO (considering El Niño, La Niña, and neutral modes) and HGE occurrence was performed by matching HGE event data as obtained from DesInventar with the E, C, and NAT-SAT indices.

3.4 | Climate and synoptic pattern analysis

We used SOM to compile the high-dimensional ERA-Interim data set from 1979 to 2013 in terms of a collection of reference vectors (i.e., cluster centroids). These vectors are organized in a low-dimensional lattice (in this case a two-dimensional regular lattice). For further details about SOMs we refer to published references (e.g., Cassano, Lynch, et al., 2006; Cassano, Uotila, et al., 2006; Hewitson & Crane, 2002; Kohonen, 2001; Reusch et al., 2007; Reusch, Alley, et al., 2005; Reusch, Hewitson, et al., 2005). In the following, we only provide details on the SOM training used in this study.

Initially, a SOM is formed by an arbitrary number of clusters or nodes. Each cluster is associated with two vectors. The first vector describes the position of the cluster on the lattice whereas the second (also called reference vector) represents the position of the cluster centroid in the data space. By using an iterative process, we then applied an unsupervised algorithm to adjust the reference vectors representing the nodes based on the differences between the reference vectors and each input value. The user determines a value (i.e., learning rate) which specifies the difference applied to each adjustment. In each cycle, the Euclidean distance between the input data and the reference vectors was calculated and the best matching reference vector was identified for each input record. Neighbouring reference vectors of each best match were then updated to result in adjacent nodes having the strongest similarity, decreasing with the distance between nodes. Iterations were ended as soon as stable values of the reference vectors were reached.

The choice of the number of nodes is subjective and depends on the specific research context and amount of data. The generalization degree of the generic patterns is thereby influenced by the number of nodes: a smaller (larger) number of nodes implies less (more) possibilities to characterize the high-dimensional data space and therefore more (less) generalization of the input data. We considered a lattice of 9 × 9 nodes because we needed a large discriminant capability to separate synoptic patterns associated with ENSO (i.e., positive, negative, and neutral phases). This decision was taken after several trainings where we identified an adequate number of nodes, following the recommendations of Gutierrez, Cano, Cofiño, and Rodriguez (2004) and Gutierrez, Cano, Cofiño, and Sordo (2005). To train the SOM, we used the MeteoLab toolbox of Matlab (MeteoLab, 2014). Input records (i.e., days) with common synoptic patterns were then linked to the same SOM node (i.e., cluster). The resulting set of clusters (i.e., Kohonen map) represents meaningful subgroups within the larger data set (i.e., generic climatic patterns). This allowed construction of frequency maps by accumulating days with the same attributes (e.g., specific E and C indices values or HGE occurrences) and their association with a specific climatic pattern. The generalized patterns in the Kohonen map were then labelled with a row-column coordinate (e.g., in Figure 3, node 9G is row 9 column G).

Outgoing long-wave radiation (OLR) anomaly was used as a proxy for convective processes (National Center for Atmospheric Research, 2014) to identify these atmospheric characteristics in the Kohonen map. OLR is a measure of the amount of energy emitted to space by earth's surface, oceans, and atmosphere. Negative (positive) OLR anomalies are indicative of enhanced (suppressed) convection and hence more (less) cloud coverage. More (less) convective activity in the central and eastern equatorial Pacific implies higher (lower), colder (warmer) cloud tops, which emit much less (more) infrared radiation into space.

4 | RESULTS

4.1 | SOM analysis of DJFMA rainfall-related variables

The Kohonen maps corresponding to the anomalies of the geopotential (Z) and specific humidity (Q) at 200 and 850 hPa show 81 possibilities of geopotential and specific humidity settings during the austral summer in this part of the globe (an overview of all Kohonen maps is provided in Figures S1–S4, Supporting information). The distribution of these 81 possibilities place antagonistic situations (i.e., El Niño and La Niña) in opposed sides of the Kohonen map and a range of intermediate possibilities in between, which are dominated by changes in the position and strength of the BH and SAH and by the variability of the SACZ at lower levels.

Frequency maps of the high anomalies of E, C, and NAT-SAT indices are presented in Figure 3. Values of E and $C > 1$ (related to eastern and central El Niño, respectively) correspond to the nodes in the column A (Figure 3a,b). However, while $E > 1$ is exclusive for A, in the case of $C > 1$ is more diffuse, over 1–4 and A–D and in the lower right part (i.e., node 9G), performing a diagonal area from top left to bottom right (Figure 3b). Values of $C < -1$ are displayed in the opposite corner, formed by column I and row 1 and along the other diagonal (i.e., from right top to left bottom) and describe the typical central La Niña phase (Figure 3c).

During the El Niño events of 1982–1983 and 1997–1998 (Figure 3a,b), 70% of the days (209 from a total of 302) were characterized by the first five nodes of the column A (El Niño corner). In contrast, the representation of the La Niña event is more diverse. Roughly 70% of the days during this phase ($C < 1$; 851 from a total of 1,212 days) are displayed in 24 nodes located in the right top to left bottom diagonal. The representation of NAT-SAT does not show a clear distribution pattern, although in the case of NAT-SAT < 1, some similarities can be found with $C > 1$ (i.e., nodes 7I, 6I, and 4I).

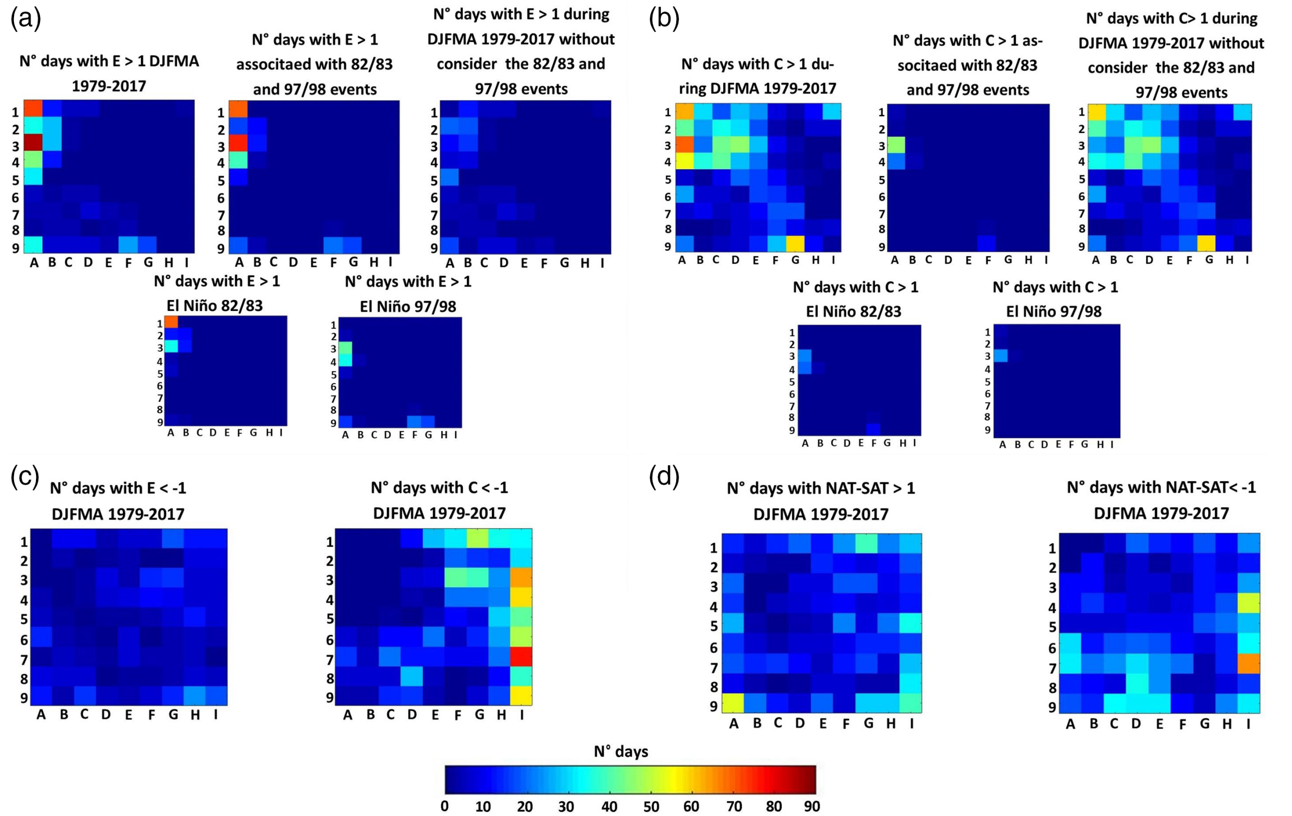

FIGURE 3 Projection of the E, C, and NAT-SAT indexes in the Kohonen map. Colours of the squares represent the number of days associated with each pattern with a specific value of the indexes. It can be observed in (a) and (b) that values of E and C above 1 are associated with nodes in the upper left corner which also correspond to El Niño patterns. On the opposite, in (c) the negative values of E and C are represented. $C < -1$ values are located in the upper right corner related with La Niña patterns while $E < -1$ values are not common and they are not displayed in a specific area of the Kohonen map [Colour figure can be viewed at wileyonlinelibrary.com]

Figure 4 illustrates OLR anomalies associated with nodes 1A, 2A, 3A, and 4A (Figure 4a, for which E and $C > 1$) and with nodes 3I, 4I, 7I, and 9I (Figure 4b, for which $C < -1$. An extra plot representing the OLR anomaly during neutral conditions (Figure 4c) is also included in order to be a reference. It is apparent that nodes in column A are clearly related with low OLR over the equatorial Pacific, describing the typical El Niño shape associated to high convection in this region, in the Ecuadorian–Colombian coast and north coast of Peru. Contrarily, nodes 3I, 4I, 7I, and 9I show high values of OLR indicating dry conditions over the equatorial Pacific as typically linked to La Niña. In tropical South America, however, negative OLR anomalies predominate, particularly in the northeast and in the tropical Andes–Amazon, featuring more convective activity over these regions during central La Niña events. Similar features can be observed directly in the Kohonen map (annex) for the specific humidity at 850 hPa, where a tongue of abnormally high (low) humidity is located just at the equator for nodes 1A, 2A, 3A, 4A (3I, 4I, 7I, 9I).

Similarly, Figures 5 and 6 represent the frequency maps of HGE records linked to specific values of E and C indices

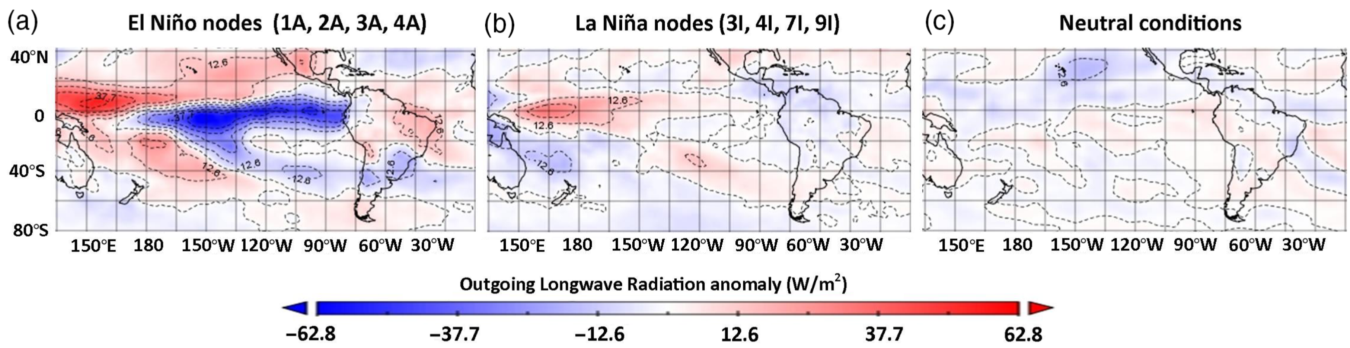

FIGURE 4 Maps representing the OLR associated with El Niño, La Niña, and neutral conditions. The neutral conditions is based in 1979 austral summer climatology which is a typical neutral year [Colour figure can be viewed at wileyonlinelibrary.com]

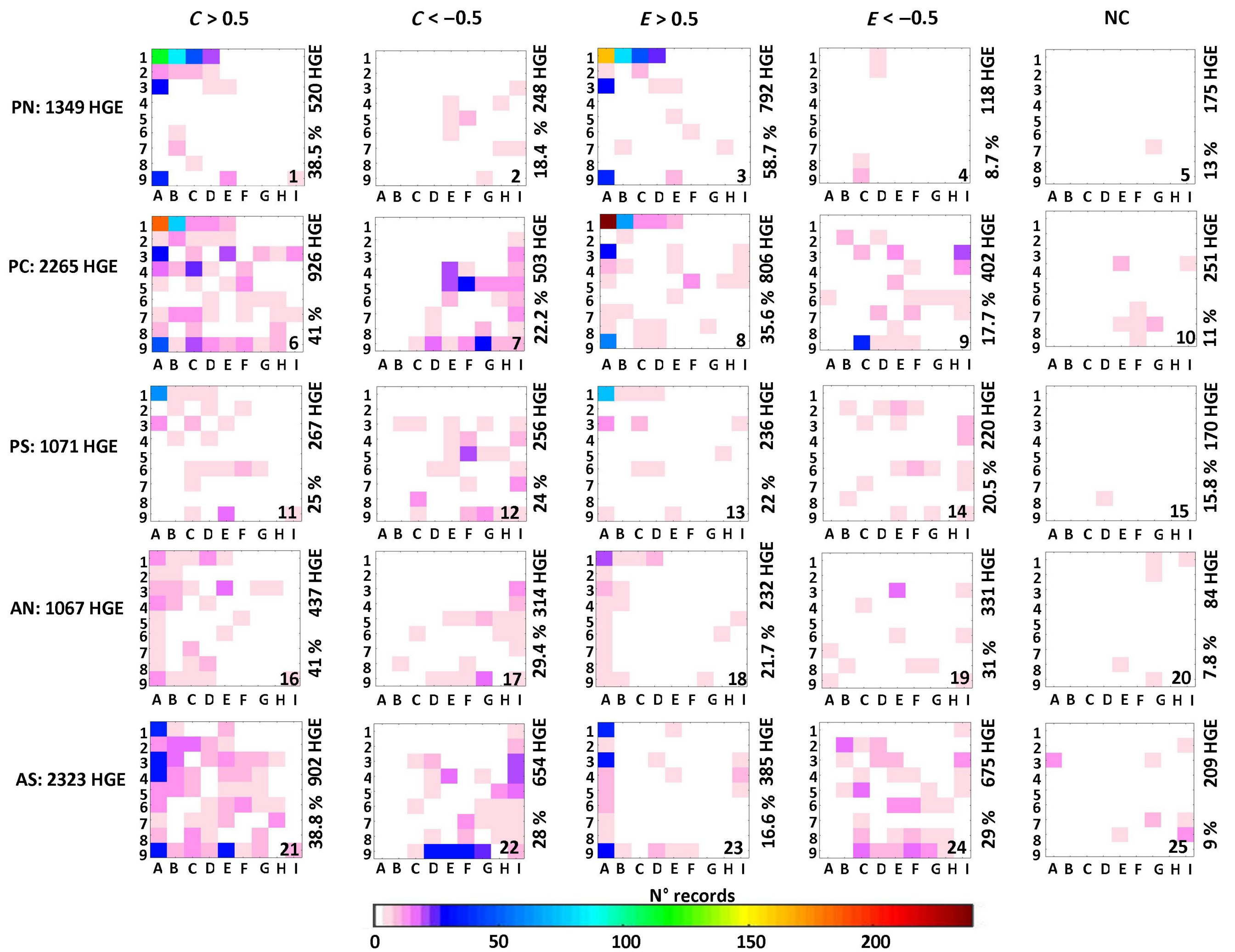

FIGURE 5 Frequency maps of HGE records linked to specific values of *E* and *C* indices in each study domain. Maps are constructed with records from December to March between 1979 and 2013. The number (and percentage linked) to the right of each map is the total of HGE records listed in DesInventar for each study area and index value between 1970 and 2013 [Colour figure can be viewed at wileyonlinelibrary.com]

in each study domain. Figure 5 includes the extreme El Niño events 82–83 and 97–98 and shows that the HGE during *C* and *E* > 0.5 are more frequent in the North and central Pacific regions of Peru. By region, in the north, more than the half part (58.7%, 792 HGE) of the total HGE is related with *E* values above 0.5 and nodes related with El Niño in the column A and row 1. In the central Pacific regions, HGE are slightly more related with *C* values above 0.5 (41%; 926 HGE). This relation between HGE and high values of *E* and *C* phenomena is less clear in the South Pacific with similar percentages of HGE associated with all the possibilities. Andean–Amazonian regions also shows high percentage of events related mainly with *C* > 0.5 (AN: 41%, 437 HGE; AS: 38.8%, 902 HGE), but they are not concentrated in specific El Niño nodes in the column A. By contrast HGE are more frequently related to *C* values <−0.5 in the South Pacific (24%, 256 HGE) and Andean–Amazonian regions of Peru (AN: 29.4%, 314 HGE; AS: 28%, 654 HGE) than in the North and central Pacific regions. These events are related with La Niña phases characterized by nodes located in the right top to left bottom diagonal of the Kohonen map. The comparison between the *E* and *C* index and the DesIventar database reveals that between 7.8 and 15.8% of HGE disasters (depending of the area) has been occurred during periods characterized by NC. Events during these conditions have been more recurring in the Pacific regions (PN: 13%, 175 HGE; PC: 11%, 251 HGE; PS: 15.8%, 170 HGE) than in the Andean–Amazonian regions (AN: 7.8%, 84 HGE; AS: 9%, 209 HGE). This information is summarized in Table 1. Figure 6 excludes the extreme events 82–83 and 97–98 showing an increment of the HGE percentages relative to NC and *C*, *E* < −0.5 as well as a decrease in the percentages of the HGE records relative to *C*, *E* > 0.5. HGE records during *E* > 0.5 are still more frequent in the North Pacific regions (42.2%, 407 HGE).

Figure 7 depicts the relative frequency of each HGE typology relative to the *C* and *E* indices. The North Pacific clearly differs from the other areas due to the high amount

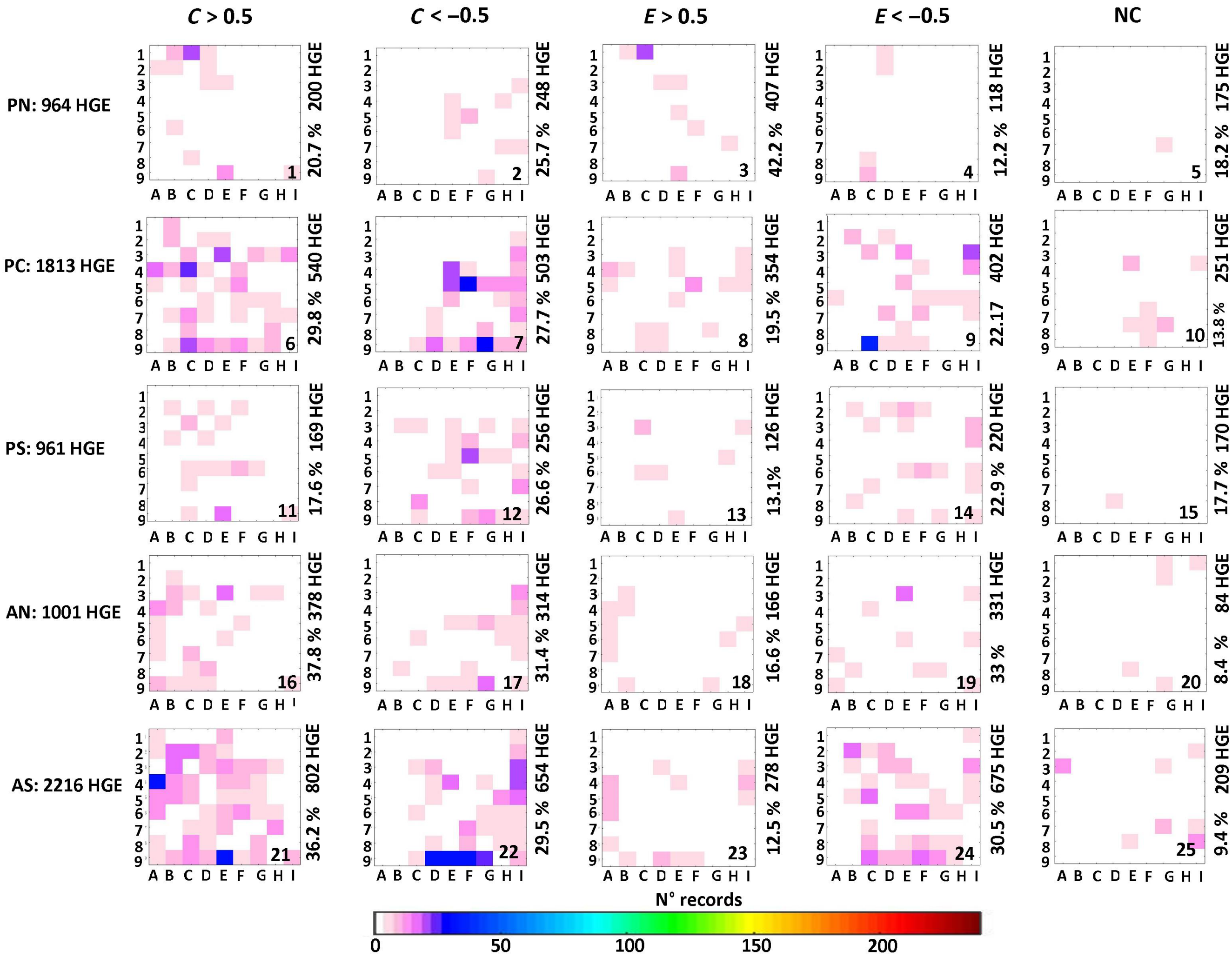

FIGURE 6 Same as Figure 5 but removing the extreme events in 1982–1983 and 1997–1998 from the analysis [Colour figure can be viewed at wileyonlinelibrary.com]

TABLE 1 Summary of the number of HGE records associated with each area and index value

Regions	Total HGE records (44 years, 1970–2013)	*C* > 0.5		*C* < −0.5		*E* > 0.5		*E* < −0.5		Neutral conditions	
		Total	%	Total	%	Total	%	Total	%	Total	%
North Pacific	1,349	520	38.5	248	18.4	792	58.7	118	8.7	175	13
Central Pacific	2,265	926	41	503	22.2	806	35.6	402	17.7	251	11
South Pacific	1,071	267	25	256	24	236	22	220	20.5	170	15.8
North Andean–Amazonia	1,067	437	41	314	29.4	232	21.7	331	31	84	7.8
South Andean–Amazonia	2,323	902	38.8	654	28	385	16.6	675	29	209	9

of HGE records related with floods and generic rainfalls, representing 86% of the cases for $C > 0.5$ and 85% for $E > 0.5$ (Table S1). In the other areas, huaycos and floods represent the majority of HGE records. Landslide records are significantly less numerous as compared to other HGE (Table S1) in the Pacific area.

4.2 | Spatio-temporal analysis of HGE

Table 2 summarizes the number of records associated to each HGE typology in the different study areas. Debris flows and flash floods were considered together since they are indistinctly denominated "huaycos" in Peru (i.e., violent displacement of a large body of water and debris, which is mobilized very fast down narrow valleys). HGE records related with floods (2,995 records) represent more than one-third of all records between 1970 and 2013, whereas debris flows and flash floods (2,174 records) and generic rainfall-related records represent one-fourth. Landslides are significantly less common (886 records). The most affected areas are in the central Pacific regions (i.e., La Libertad, Ancash, and Lima) and in south Andean–Amazonian (i.e., Apurimac, Cusco, Huancavelica, and Junín). Figure 8 and Table 3 show the distribution of HGE records for each year and zone in

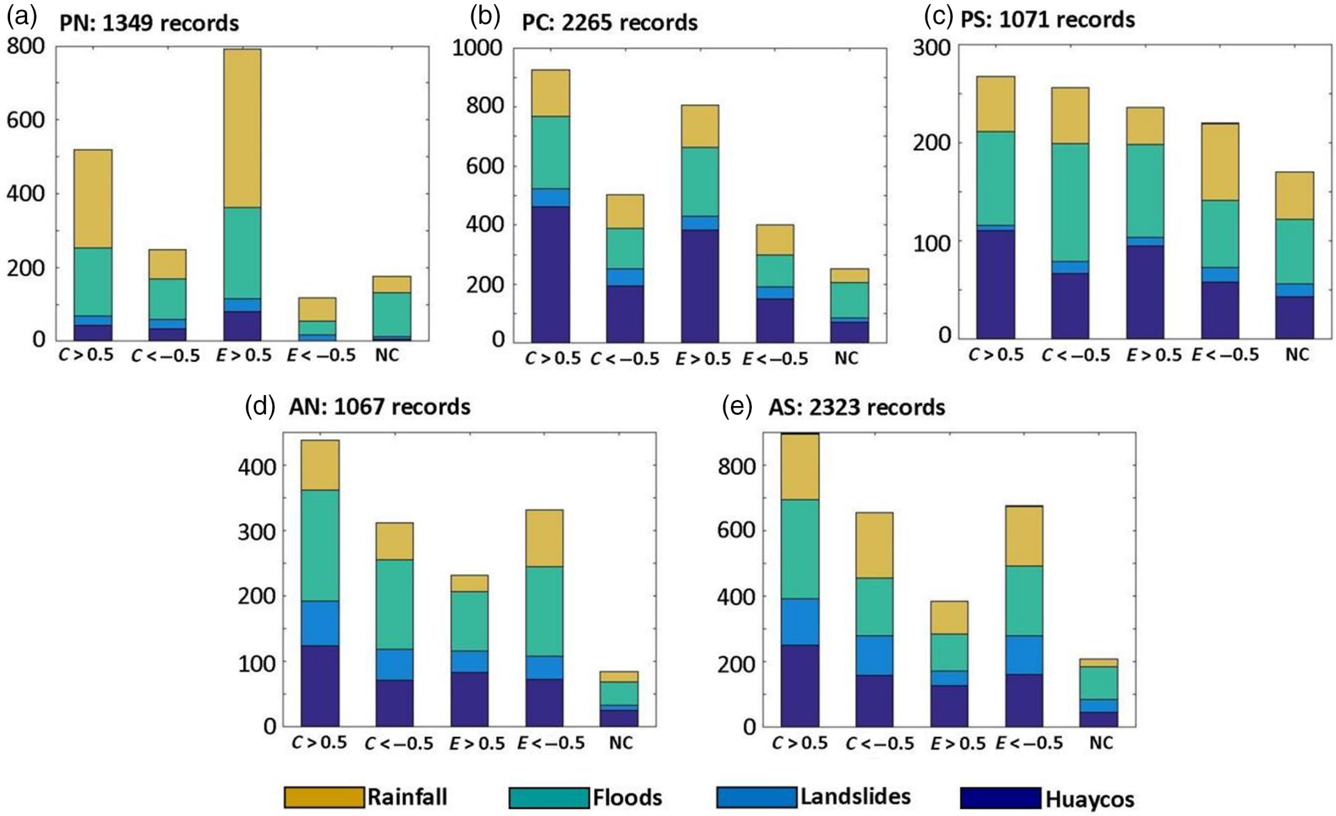

FIGURE 7 Plots representing the number of records associated to each area and related to the *E* and *C* indices between 1970 and 2013. Quantitative information is summarized in Table S1 [Colour figure can be viewed at wileyonlinelibrary.com]

TABLE 2 Summary of the number of records by typology and study area. Predominant HGE records are overall related with floods, flash floods, and debris flows

	Landslides	Floods	Huaycos	Rainfall
North Pacific	73	557	103	616
Central Pacific	191	736	928	409
South Pacific	57	458	293	263
North Andean–Amazonia	152	449	277	190
South Andean–Amazonia	413	795	573	537
Total: 8,043	886 (11%)	2,995 (37.2%)	2,174 (26.7%)	2,015 (25%)

relation to the *C*, *E* and NAT-SAT (DJFMA average values) indices. Very positive values of *E* define the strong El Niño events in 1972–1973, 1982–1983, 1997–1998, and 2015–2016. Temporal analysis of events recorded in the DesInventar database points to peaks in HGE occurrences during these episodes overall in the North–central Pacific regions (Figure 8a,b and Table 3) and more smoothly in the South Pacific regions (Figure 8c). HGE in Andean–Amazonian regions (Figure 8d,e) do not show relation with El Niño events, except in the south Amazonian regions with the El Niño event in 1973. By contrast, in the southern Amazonian regions, there is a match between HGE with negative values of *C* (related with La Niña phenomena) and NAT-SAT indices (Figure 8e and Table 3). In no instance do we observe any clear temporal tendency in the HGE occurrence for the entire period (1970–2013). South Andean–Amazonian regions exhibit the highest number of HGE records (2,323 HGE) together with the central Pacific regions (2,265 HGE) accounting for almost 30% of the total events (8,075 HGE) (Table 3).

Figure 9 shows the distribution of HGE records per region. The red line indicates the population of each region. The number of HGE disasters provided in the DesInventar database is mainly clustered around Lima, Huánuco, and Cuzco, as well as around Piura, Ancash, and Arequipa. There is no clear HGE geographical preference between the regions (i.e., either from north to south or from the mountains to the coast).

5 | DISCUSSION AND CONCLUSIONS

In this article we provide insights into the relation between the occurrence of HGE in the most populated

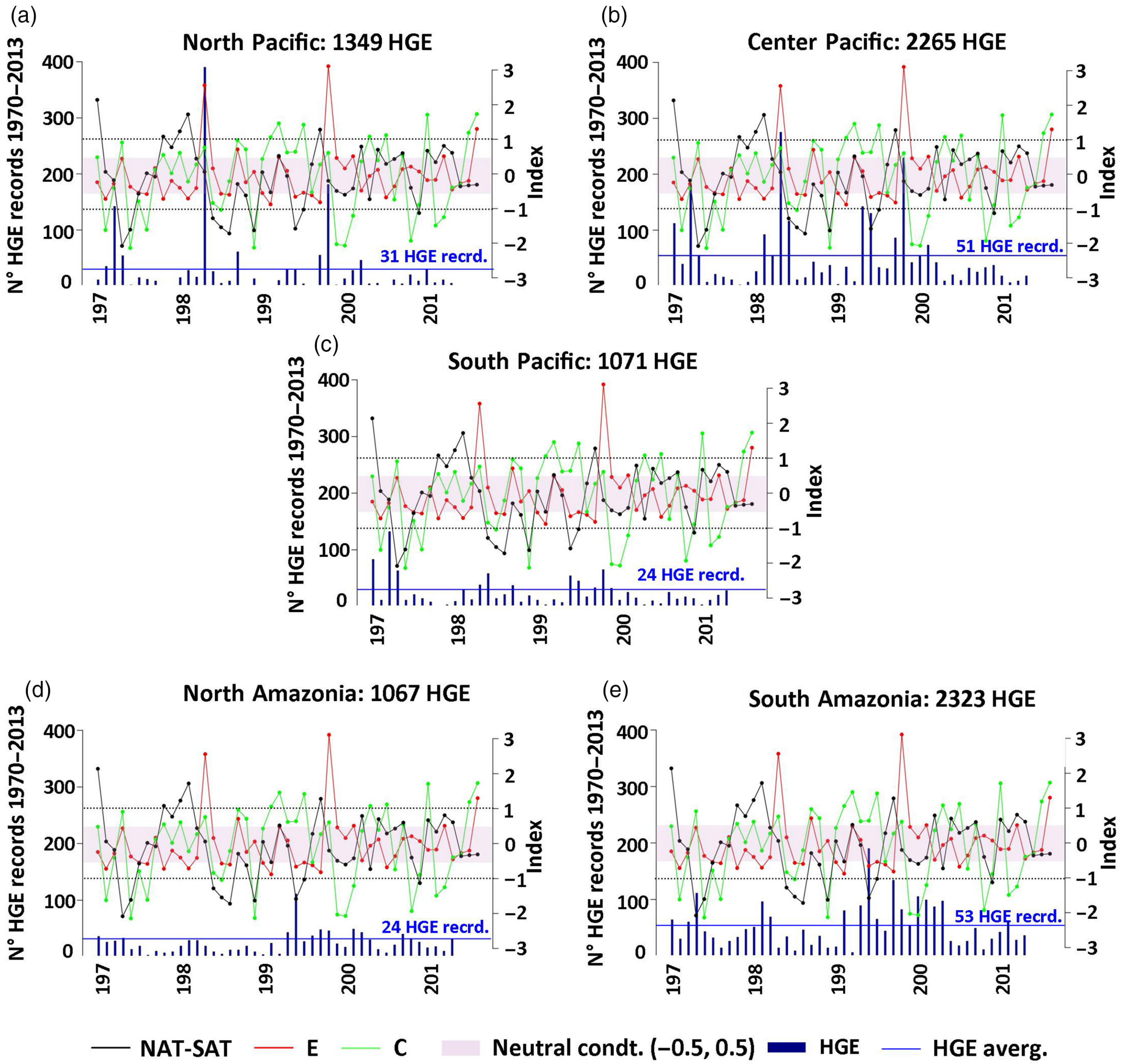

FIGURE 8 HGE occurrences at inter-annual timescale between 1970 and 2013 for each study area. The HGE are confronted with the *E*, *C*, and NAT-SAT indexes. High values of *E* (red line) represent the two big El Niño events in 1982/1983, 1997/1998, and 2015/2016. The number of HGE records is strongly related with these events in the North and central Pacific regions. Negative values of *C* under 1 represent La Niña events which are more correlated with HGE records overall in the south Amazonian regions [Colour figure can be viewed at wileyonlinelibrary.com]

areas of Peru and the climatic conditions during austral summers. We applied SOM to characterize the synoptic patterns of HGE occurrences in Peru over the past 35 years. Our results clearly highlight that a substantial number (36%) of hydro-geomorphic disasters along the Peruvian coast and in the Andean–Amazonian regions are not related to the occurrence of El Niño phenomena, while 36% of the events are related to La Niña or neutral conditions. The fact that HGEs occur during a large fraction of non-El Niño conditions emphasizes the need to better understand and analyse these events and their drivers as well.

This study is based on the DesInventar data set, mainly containing information from newspaper items published in "El Comercio." This database is considered to be the most complete for the region based on its temporal and spatial resolution (DesInventar, 2015; Huggel et al., 2015). However, we are aware that some HGE events may have been missed due to the nature of the database sources. In fact, the coverage of newspaper reports varies across the country (Huggel et al., 2015). Consequently, a potential bias cannot be entirely ruled out. The database presents higher frequency of events reported in the major cities of Peru (i.e., mainly around Lima, Huánuco, and Cuzco, but also

TABLE 3 Summary of the distribution of events per study area. Total HGE records are between 1970 and 2013. Highlighted years represent more than twice the average values. Red (blue) dates are related to strong El Niño (La Niña) events. 1994 events are not related with SST anomalies in the equatorial Pacific but they are coincident with a negative value of NAT-SAT index

	Total HGE records (44 years, 1970–2013)	Percentage	HGE average per year	Highlighted years above average
North Pacific	1,349	16.7%	31	1972, 1983, 1998
Central Pacific	2,265	28%	51	1970, 1972, 1983, 1984, 1993, 1994, 1998
South Pacific	1,071	13.3%	24	1970, 1972
North Andean–Amazonia	1,067	13.2%	24	1994
South Andean–Amazonia	2,323	28.8%	53	1973, 1994, 1997, 2000
Total	8,075			

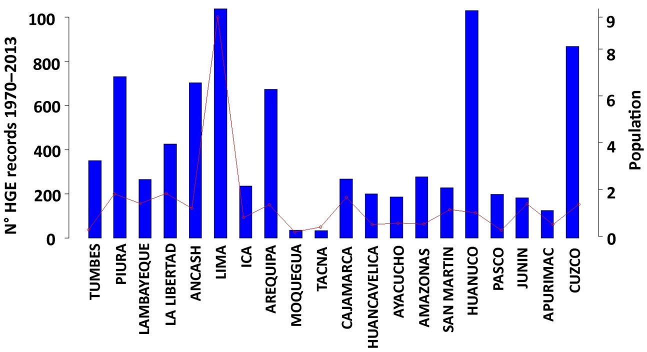

FIGURE 9 Overview of existing HGE records per region. Regions are arranged from left to right in a north–south direction. The number of HGE records is highest in Lima, Cuzco, and Huánuco. The red line indicates the population of each region; no clear relationship exists between population density and the occurrence of HGE. North Pacific: Tumbes, Piura, and Lambayeque. Central Pacific: Libertad, Ancash, and Lima. South Pacific: Ica, Arequipa, Moquegua, Tacna, Huancavelica, and Ayacucho. North Andean Amazonas: Amazonas, Cajamarca, san Martin, Huánuco, and Pasco. South Andean Amazonas: Apurimac, Cusco, Huancavelica, and Junin [Colour figure can be viewed at wileyonlinelibrary.com]

around Piura, Ancash, and Arequipa), which are important economic centres with large populations and much infrastructure at risk. The variability in the number of HGE records in relation to the political regions clearly influences our results about the relationship between HGE and climatic indices. Thus, in Figures 5 and 8, the big amount of HGE records in the central Pacific regions (i.e., 2,265 HE records) is due to the presence of Lima in this study area. In fact, if we remove the records associated with Lima from the analysis of Figure 5 (Figure S5; plots 6–10 showing the decrease in the HGE values comparing to same plots in Figure 5), we find a more realistic image of the rainfall regime in the central Pacific regions (i.e., this region corresponds to the driest region in the country without relationship between strong rainfall peaks and strong ENSO events (Rau et al., 2017).

Considering the above, the DesInventar database has nevertheless served as useful tool to display the spatio-temporal coherence with ENSO phenomena. Thus, the database allows to draw conclusions about the dissimilar effect of different types of El Niño along Peru, with more costal El Niño-triggered HGE disasters in the north coast of the country and progressively less towards the south and interior highlands. These dissimilar consequences were evident during El Niño 2015–2016 when an extreme drought was reported in the western Amazon and Andean regions while the northern Peru experienced above-average rainfalls triggering several floods, flash-floods, and landslides (Marengo, Espinoza, Alvez, Ronchail, & Baez, 2017). The opposite situation is observed during the central La Niña-like mode (i.e., $C < -0.5$) and therefore confirms previous observations based on rainfall anomalies (Lavado-Casimiro & Espinoza, 2014; Sulca et al., 2017).

We have identified HGE occurring during El Niño, La Niña, and neutral conditions based on the *E* and *C* indices (Takahashi et al., 2011). Thus, in the north and central regions of the Pacific coast, the occurrence of HGE is related to SST variability over the north coast of Peru, which is represented by the *E* index. Positive SST anomalies in this region (*E* values >0.5) are related to more than half (58.7%) of the HGE in the North Pacific regions, and to 35.6% in the central Pacific regions (Figure 5 plots 3 and 8). On the other hand, the situation in the central Pacific Ocean seems to play a key role in the occurrence of HGE in the central (PC) and south (PS) regions of the Pacific coast as well as in the Andean–Amazonian regions. Both negative and positive SST anomalies, represented by *C* index, seems to control a big percentage of HGE here: positive values ($C > 0.5$, in combination with positive values of *E*) count for close to 40% of all HGE in the areas (except for the South Pacific regions), whereas negative values ($C < -0.5$) are related with almost one third of all HGE occurring in the Andean–Amazonian regions. This result agrees with previous studies describing rainfall variability over the Amazonas basin, linking stronger-than-normal rainfalls with La Niña episodes (Espinoza, Ronchail, Frappart, et al., 2013; Espinoza Villar et al., 2009; Lavado-Casimiro & Espinoza, 2014; Marengo, 1992; Marengo, Tomasella, & Uvo, 1998; Richey, Nobre, & Deser, 1989). Besides, some peaks of HGE in the Andean–Amazonian regions are coincident with strong negative values of NAT-SAT (e.g., Figures 8, 1973 in south Amazonia regions and 1994 in north/south Amazonia regions). This finding concurs with results from Espinoza Villar et al. (2009) and Lavado-Casimiro et al. (2013), who demonstrated that at inter-annually timescales, rainfall fluctuations over the Amazon basin are related to SST gradient variability in the tropical Atlantic during summers. In fact, rainfall is more abundant when the SST in the north tropical Atlantic is lower than the SST in the south tropical Atlantic, thus implying negative values of NAT-SAT. Interestingly, although HGE occurring during neutral conditions (i.e., *E*, *C*, and NAT-SAT values range between −0.5 and 0.5) show the lowest percentages, they were well represented in all regions across Peru, with values ranging between 7.8 and 15.8% of the total. We assume that HGE during neutral conditions are related to (a) local-scale atmospheric events and to (b) large-scale synoptic features. Our approach using SOM recognizes only the main large-scale features during the South American austral summer. In general, the austral summer precipitation over the Peruvian central Andes is related to mid- and upper-level easterly winds supported by a strengthening of the Bolivian High, leading to an influx of warm, moist air from the Amazon basin into the central Andes that feeds convective storms (Garreaud, 1999, 2000; Garreaud et al., 2003; Segura et al., 2016; Sulca et al., 2016; Vuille, 1999; Vuille et al., 2000; Vuille & Keimig, 2004). However, shorter rainfall events in the Peruvian central Andes and the Altiplano can occur during the austral summer as well, and are related to fluctuations in the strength and position of this high-pressure system and the SACZ (Lenters & Cook, 1999; Sulca et al., 2016). As recently explained by Sulca et al. (2016), wet events in the Peruvian central Andes are related to an upper-level anticyclone (associated with a cyclonic anomaly over southern South America) which strengthens upper-level easterly winds on its northern flank, thereby setting the stage for wet events by transporting moist air from the Amazon basin. On the other hand, under neutral conditions, coastal regions are influenced by the southern Pacific anticyclone and the Humboldt Current, thereby generating dry conditions and extreme aridity (Lavado Casimiro et al., 2012; Rau et al., 2017; Vuille et al., 2000). Knowledge about the relation between rainfall events in this region during neutral conditions and austral summer large-scale circulation over South America is still very poor; it is assumed to be related to the southwards shift of the ITCZ and to mechanisms influencing atmospheric processes over the Peruvian Andes (i.e., moist air transports from the Amazon, Bolivian High) (Lagos et al., 2008; Nickl, 2007; Rau et al., 2017).

Regardless of the intensity and climatic origin of the HGE, all recorded HGE in DesInventar have had a negative impact on Peruvian society because of pre-existing vulnerabilities (Cutter, 1996). In Peru, vulnerabilities to natural hazards are amplified by several factors like poverty, inappropriate location of settlements, rapid and unplanned urbanization, or improper construction of homes, among others (McEntire & Fuller, 2002; Young & León, 2009). In a context where 21.8% of the population is living under poverty conditions, we paid special attention to the 69% of this poor population located in mountainous areas (Instituto Nacional de Estadística e Informática, 2016), since 42% of all HGE analysed in this work have been recorded in mountain regions. Poverty is a key factor in the vulnerability to natural disasters (Hallegate, Vogt-Schilb, Bangalore, Rozenberg, 2017), especially in these areas which are characterized by inaccessibility, fragility, or marginality, which all constrain human activities (Jodha, 1992, 1997, 2001; Körner & Ohsawa, 2005). Any improvement in the disaster management strategies in these regions and in the rest of the country should also include events taking place during different ENSO phases (i.e., El Niño, La Niña, and neutral conditions) as well as during other climatic modes. For example, results observed in Figure 6, where we exclude only 2 years characterized by the extreme El Niño events in 1982–1983 and 1997–1998, highlight the relevance of the impacts related to La Niña and neutral conditions in Peru. Even if recorded damage during these phases is lower than during El Niño, they are not at all negligible. In fact, damage related to HGE occurring during La Niña and neutral condition accounted for more than US$40 million in economic losses and more than 2,000 fatalities between 1970 and 2013.

We conclude that the occurrence of HGE in Peru is independent of ENSO phases at the regional scale. However, more work is needed to estimate rainfall thresholds for local processes and areas regarding their geological, physiographic, and land use settings. Such research remains, however, challenging because of the generalized lack of systematic rainfall data in many areas of Peru. Here, satellite products (e.g., satellite precipitation data from the TRMM TMPA-RT product; Huffman et al., 2007; Huffman, Adler, Bolvin, & Nelkin, 2010) represent a new opportunity to complement rainfall data in regions where this information is too scarce to capture spatial precipitation patterns (Cabrera, Yupanquib, & Raub, 2016; Chavez & Takahashi, 2017; Espinoza et al., 2016; Lavado-Casimiro, Labat, Guyot, Ronchail, & Ordoñez, 2009; Manz et al., 2016).

ACKNOWLEDGEMENTS

The authors are grateful to the PACC project and the Swiss Agency for Development and Cooperation (SDC) for partial funding of this study. We acknowledge the Santander Meteorology Group for their open source Matlab toolbox (MeteoLab) used for statistical (data mining) analysis and especially S. Herrera for his technical support. The authors wish to thank all the reviewers whose comments and suggestions considerably helped to improve the manuscript.

ORCID

J. C. Espinoza http://orcid.org/0000-0001-7732-8504
M. Stoffel http://orcid.org/0000-0003-0816-1303

REFERENCES

Alvarez, M. S., Vera, C. S., Kiladis, G. N., & Liebmann, B. (2016). Influence of the Madden Julian oscillation on precipitation and surface air temperature in South America. *Climate Dynamics*, *46*(1–2), 245–262. https://doi.org/10.1007/s00382-015-2581-6

Ashok, K., Behera, S. K., Rao, S. A., Weng, H., & Yamagata, T. (2007). El Niño Modoki and its possible teleconnection. *Journal of Geophysical Research*, *112*, C11007. https://doi.org/10.1029/2006JC003798

Barnston, A., & Livezey, R. E. (1987). Classification, seasonality, and persistence of low-frequency circulation patterns. *Monthly Weather Review*, *115*, 1083–1126.

Barreiro, M., Chang, P., & Saravanan, R. (2002). Variability of the South Atlantic convergence zone simulated by an atmospheric general circulation model. *Journal of Climate*, *15*, 745–763.

Barry, R. G., & Carleton, A. M. (2001). *Synoptic and dynamic climatology*. New York, NY: Routledge.

Bayer, A. M., Danysh, H. E., Garvich, M., Gonzálvez, G., Checkley, W., Alavarez, M., & Gilman, R. H. (2014). An unforgettable event: A qualitative study of the 1997–98 El Niño in northern Peru. *Disasters*, *38*(2), 351–374.

Berrisford, P., Dee, D. P., Fielding, K., Fuentes, M., Kallberg, P., Kobayashi, S., & Uppala, S. (2009). *The ERA-Interim archive* (ERA Report No. 1). Reading, England: ECMWF.

Brönnimann, S. (2007). Impact of El Niño–Southern Oscillation on European climate. *Reviews of Geophysics*, *45*, RG3003. https://doi.org/10.1029/2006RG000199

Buell, C. E. (1975). *The topography of empirical orthogonal functions.* Paper presented at the fourth conference on probability and statistics in atmospheric sciences, American Meteorological Society, Tallahassee, FL.

Cabrera, J., Yupanquib, R., & Raub, P. (2016). Validation of TRMM daily precipitation data for extreme events analysis. The case of Piura watershed in Peru. *Procedia Engineering*, *154*, 154–157.

Cai, W., Borlace, S., Lengaigne, M., van Rensch, P., Collins, M., Vecchi, G., … Jin, F. F. (2014). Increasing frequency of extreme El Niño events due to greenhouse warming. *Nature Climate Change*, *4*, 111–116. https://doi.org/10.1038/nclimate2100

Carvalho, L., Jones, C., & Liebmann, B. (2004). The South Atlantic convergence zone: Intensity, form, persistence, and relationships with intraseasonal to interannual activity and extreme rainfall. *Journal of Climate*, *17*, 88–108.

Cassano, E. N., Lynch, A. H., Cassano, J. J., & Koslow, M. R. (2006). Classification of synoptic patterns in the western Arctic associated with extreme events at Barrow, Alaska, USA. *Climate Research*, *30*(2), 83–97.

Cassano, J. J., Uotila, O., & Lynch, A. (2006). Changes in synoptic weather patterns in the polar regions in the 20th and 21st centuries, part 1: Arctic. *International Journal of Climatology*, *26*, 1027–1049.

Cassano, J. J., Uotilla, P., Lynch, A. H., & Cassano, E. N. (2007). Predicted changes in synoptic forcing of net precipitation in large Arctic River basins during the 21st century. *Journal of Geophysical Research*, *112*, G04S49. https://doi.org/10.1029/2006JG000332

Cavalcanti, I., Marengo, J., Alves, L., & Costa, D. (2016). On the opposite relation between extreme precipitation over west Amazon and southeastern Brazil: Observations and model simulations. *International Journal of Climatology*, *37*(9), 3606–3618. https://doi.org/10.1002/joc.4942

Chavez, S. P., & Takahashi, K. (2017). Orographic rainfall hotspots in the Andes–Amazon transition according to the TRMM precipitation radar and in situ data. *Journal of Geophysical Research: Atmospheres*, *122*, 5870–5882. https://doi.org/10.1002/2016JD026282

Cohen, S. J. (1983). Classification of 500 mb height anomalies using obliquely rotated principal components. *Journal of Applied Meteorology*, *12*, 1975–1988.

Comunidad Andina. (2008). Pérdidas por desastres en Perú entre 1970–2006. Retrieved from http://www.comunidadandina.org/predecan/doc/r2/osso/Cons025-2006-CorporacionOSSO-Articulo-Peru.pdf

CPC/IRI. (2016). El Niño/Southern Oscillation (ENSO). Diagnostic discussion. Retrieved from http://www.cpc.noaa.gov/products/expert_assessment/ENSO_DD_archive.shtml

Cutter, S. L. (1996). Vulnerability to environmental hazards. *Progress in Human Geography*, *20*(4), 529–539.

Cutter, S. L., Barnes, L., Berry, M., Burton, C., Evans, E., Tate, E., & Webb, J. (2008). A place-based model for understanding community resilience to natural disasters. *Global Environmental Change*, *18*, 598–606.

Cutter, S. L., & Finch, C. (2008). Temporal and spatial changes in social vulnerability to natural hazards. *Proceedings of the National Academy of Sciences of the United States of America*, *105*, 2301–2306.

De Souza, E. B., & Ambrizzi, T. (2006). Modulation of the intraseasonal rainfall over tropical Brazil by the Madden–Julian oscillation. *International Journal of Climatology*, *26*, 1759–1776.

Dee, D. P., Uppala, S. M., Simmons, A. J., Berrisford, P., Poli, P., Kobayashi, S., … Vitart, F. (2011). The ERA-Interim reanalysis: Configuration and performance of the data assimilation system. *Quarterly Journal of the Royal Meteorological Society*, *137*, 553–597.

DesInventar. (2015). *DesInventar—Inventory system of the effects of disasters.* Cali, Colombia: Corporación OSSA. Retrieved from http://desinventar.org

Dewitte, B., Takahashi, K., Goubanova, K., Montecinos, A., Mosquera, K., Illig, S., … Espinoza, J. C. (2014). Las diversas facetas de El Niño y sus efectos en la costa del Perú. In I. Montes (Ed.), *El peru frente al cambio climatico* (pp. 125–140). Lima, Peru: MINAM-IRD.

Diaz, A., & Aceituno, P. (2003). Atmospheric circulation anomalies during episodes of enhanced and reduced convective cloudiness over Uruguay. *Journal of Climate*, *16*, 3171–3185.

Enfield, D., Mestas-Nuñez, A., Mayer, D., & Cid-Serrano, L. (1999). How ubiquitous is the dipole relationship in tropical Atlantic sea surface temperatures? *Journal of Geophysical Research: Oceans*, *104*(C4), 7841–7848. https://doi.org/10.1029/1998jc900109

Espinoza, J. C., Segura, H., Ronchail, J., Drapeau, G., & Gutierrez-Cori, O. (2016). Evolution of wet- and dry-day frequency in the western Amazon basin: Relationship with atmospheric circulation and impacts on vegetation. *Water Resources Research*, *52*, 8546–8560. https://doi.org/10.1002/2016WR019305

Espinoza, J. C., Lengaigne, M., Ronchail, J., & Anicot, S. (2012). Large-scale circulation patterns and related rainfall in the Amazon Basin: A neuronal networks approach. *Climate Dynamics*, *38*(1–2), 121–140. https://doi.org/10.1007/s00382-011-1010-8

Espinoza, J. C., Marengo, J., Ronchail, J., Carpio, J., Flores, L., & Guyot, J. (2014). The extreme 2014 flood in south-western Amazon basin: The role of tropical–subtropical South Atlantic SST gradient. *Environmental Research Letters*, *9*(12), 124007. https://doi.org/10.1088/1748-9326/9/12/124007

Espinoza, J. C., Ronchail, J., Frappart, F., Lavado, W., Santini, W., & Guyot, J. L. (2013). The major floods in the Amazonas River and tributaries (western Amazon basin) during the 1970–2012 period: A focus on the 2012 flood. *Journal of Hydrometeorology*, *14*, 1000–1008. https://doi.org/10.1175/JHM-D-12-0100.1

Espinoza, J. C., Ronchail, J., Guyot, J., Junquas, C., Vauchel, P., Lavado, W., … Pombosa, R. (2011). Climate variability and extreme drought in the upper Solimões River (western Amazon Basin): Understanding the exceptional 2010 drought. *Geophysical Research Letters*, *38*(13), L13406. https://doi.org/10.1029/2011gl047862

Espinoza, J. C., Ronchail, J., Lengaigne, M., Quispe, N., Silva, Y., Bettolli, M., … Llacza, A. (2013). Revisiting wintertime cold air intrusions at the east of the Andes: Propagating features from subtropical Argentina to Peruvian Amazon and relationship with large-scale circulation patterns. *Climate Dynamics*, *41*(7–8), 1983–2002. https://doi.org/10.1007/s00382-012-1639-y

Espinoza Villar, J. C., Guyot, J., Ronchail, J., Cochonneau, G., Filizola, N., Fraizy, P., … Auchel, P. (2009). Contrasting regional discharge evolutions in the Amazon basin (1974–2004). *Journal of Hydrology*, *375*(3–4), 297–311. https://doi.org/10.1016/j.jhydrol.2009.03.004

European Centre for Medium-Range Weather Forecasts. (2016). *ERA-Interim daily data.* Retrieved from http://apps.ecmwf.int/datasets/data/interim-full-daily/levtype=sfc/

Falvey, M., & Garreaud, R. (2005). Moisture variability over the South American Altiplano during the SALLJEX observing season. *Journal of Geophysical Research*, *110*, D22105. https://doi.org/10.1029/2005JD006152

Fernandes, K., Baethgen, W., Bernardes, S., DeFries, R., DeWitt, D., Goddard, L., … Uriarte, M. (2011). North tropical Atlantic influence on western Amazon fire season variability. *Geophysical Research Letters*, *38*(12), L12701. https://doi.org/10.1029/2011gl047392

Figueroa, S. N., Satyamurty, P., & Da Silva Dias, P. L. (1995). Simulations of the summer circulation over the South American region with an eta coordinate model. *Journal of the Atmospheric Sciences*, *52*, 1573–1584.

Frey, H., Huggel, C., Bühler, Y., Buis, D., Burga, M. D., Choquevilca, W., … Walser, M. (2016). A robust debris-flow and GLOF risk management strategy for a data-scarce catchment in Santa Teresa, Peru. *Landslides*, *13*, 1493–1507. https://doi.org/10.1007/s10346-015-0669-z

Garreaud, R. (1999). Multiscale analysis of the summertime precipitation over the central Andes. *Monthly Weather Review*, *127*(5), 901–921. https://doi.org/10.1175/1520-0493(1999)127<0901:maotsp>2.0.co;2

Garreaud, R. (2000). Intraseasonal variability of moisture and rainfall over the South American Altiplano. *Monthly Weather Review*, *128*(9), 3337–3346. https://doi.org/10.1175/1520-0493(2000)128<3337:ivomar>2.0.co;2

Garreaud, R., Vuille, M., & Clement, A. (2003). The climate of the Altiplano: Observed current conditions and mechanism of past changes. *Palaeogeography, Palaeoclimatology, Palaeoecology*, *194*(3054), 1–18.

Garreaud, R. D., Vuille, M., Compagnucci, R., & Marengo, J. (2009). Present-day South American climate. *Palaeogeography, Palaeoclimatology, Palaeoecology*, *281*, 180–195.

Glantz, M. H. (2001). *Once burned, twice shy? Lessons learned from the 1997–98 El Niño*. Tokyo, Japan: United Nations University Press.

Gutierrez, J. M., Cano, R., Cofiño, A. S., & Rodriguez, M. A. (2004). Clustering methods for statistical downscaling in short-range weather forecast. *Monthly Weather Review*, *132*, 2169–2183.

Gutierrez, J. M., Cano, R., Cofiño, A. S., & Sordo, C. (2005). Analysis and downscaling multi-model seasonal forecasts in Peru using self-organizing maps. *Tellus Series A: Dynamic Meteorology and Oceanography*, *57*, 435–447.

Hallegate, S., Vogt-Schilb, A., Bangalore, M., Rozenberg, J. (2017). *Unbreakable: Building the resilience of the poor in the face of natural disasters Climate change and development series*. Washington, DC: World Bank. https://doi.org/10.1596/978-1-4648-1003-9

Hewitson, B., & Crane, R. (2002). Self-organizing maps: Applications to synoptic climatology. *Climate Research*, *22*, 13–26.

Hong, Y., Hsu, K., Sorooshian, S., & Gao, X. (2005). Self-organizing nonlinear output (SONO): A neural network suitable for cloud patch-based rainfall estimation at small scales. *Water Resources Research*, *41*, W03008. https://doi.org/10.1029/2004WR003142

Huffman, G. J., Adler, R. F., Bolvin, D. T., Gu, G., Nelkin, E. J., Bowman, K. P., … Wolff, D. B. (2007). The TRMM multisatellite precipitation analysis (TMPA): Quasi-global, multiyear, combined-sensor precipitation estimates at fine scales. *Journal of Hydrometeorology*, *8*, 38–55. https://doi.org/10.1175/JHM560.1

Huffman, G. J., Adler, R. F., Bolvin, D. T., & Nelkin, E. J. (2010). The TRMM multi-satellite precipitation analysis (TMPA). In F. Hossain & M. Gebremichael (Eds.), *Satellite rainfall applications for surface hydrology* (pp. 3–22). Dordrecht, Netherlands: Springer.

Huggel, C., Raissig, A., Rohrer, M., Romero, G., Diaz, A., & Salzmann, N. (2015). How useful and reliable are disaster databases in the context of climate and global change? A comparative case study analysis in Peru. *Natural Hazards and Earth System Sciences*, *15*, 475–485.

Hurrell, J. W., Kushnir, Y., Ottersen, G., & Visbeck, M. (2003). *The North Atlantic Oscillation: Climate significance and environmental impact* (Vol. 134, 279 pp.) *Geophysical monograph series*. Washington, DC: American Geophysical Union.

Instituto Nacional de Defensa Civil. (2010). Informe de emergencia N° 056. Retrieved from http://www.indeci.gob.pe

Instituto Nacional de Defensa Civil. (2017). Resúmen ejecutivo—Temporada de lluvias Diciembre 2016–Marzo 2017. Retrieved from http://www.indeci.gob.pe/objetos/alerta/MjYxNg==//20170330165025.pdf

Instituto Nacional de Estadística e Informática. (2016). *Informe técnico: Evolución de la Pobreza Monetaria, 2009–2015.* Lima, Peru: Author.

Jodha, N. S. (1992). Mountain perspective and sustainability: A framework for development strategies. In N. S. Jodha, M. Banskota, & T. Partap (Eds.), *Sustainable mountain agriculture: Perspectives and issues* (Vol. *1*, pp. 41–82). New Delhi, India: Oxford and IBH.

Jodha, N. S. (1997). Mountain agriculture. In B. Messerli & J. D. Ives (Eds.), *Mountains of the world: A global priority* (pp. 331–335). New York, NY; Carnforth, England: The Parthenon Publishing Group.

Jodha, N. S. (2001). Interacting processes of environmental vulnerabilities mountain areas. *Issues in Mountain Development*, *2001/2*, 1–6.

Johnson, N. C., Feldstein, S. B., & Tremblay, B. (2008). The continuum of Northern Hemisphere teleconnection patterns and a description of the NAO shift with the use of self-organizing maps. *Journal of Climate*, *21*, 6354–6371.

Jolliffe, I. T. (2002). *Principal component analysis*. New York, NY: Springer.

Junquas, C., Takahashi, K., Condom, T., Espinoza, J. C., Chavez, S., Sicart, J. E., & Lebel, T. (2017). Understanding the influence of orography on the precipitation diurnal cycle and the associated atmospheric processes in the central Andes. *Climate Dynamics*. https://doi.org/10.1007/s00382-017-3858-8

Kodama, Y. (1992). Large-scale common features of subtropical precipitation zones (the Baiu frontal zone, the SPCZ and the SACZ), part I: Characteristics of subtropical frontal zones. *Journal of the Meteorological Society of Japan*, *70*(4), 813–836.

Kodama, Y., Sagawa, T., Ishida, S., & Yoshikane, T. (2012). Roles of the Brazilian Plateau in the formation of the SACZ. *Journal of Climate*, *25*, 1745–1758.

Kohonen, T. (2001). *Self-organizing maps*. New York, NY: Springer.

Körner, C., & Ohsawa, M. (2005). Mountain systems. In R. Hassan, R. Scholes, & N. Ash (Eds.), *Ecosystems and human well-being: Current state and trends. Millennium ecosystem assessment* (Vol. 1, pp. 681–716). Washington, DC: Island Press.

Kousky, V. E. (1979). Frontal influences on northeast Brazil. *Monthly Weather Review*, *107*, 1140–1153.

Kug, J. S., Jin, F. F., & An, S. I. (2009). Two types of El Niño events: Cold tongue El Niño and warm pool El Niño. *Journal of Climate*, *22*, 1499–1515. https://doi.org/10.1175/2008JCLI2624.1

Kutzbach, J. E. (1967). Empirical eigenvectors of sea-level pressure, surface temperature and precipitation complexes over North America. *Journal of Applied Meteorology*, *6*, 791–802.

L'Heureux, M. L., Takahashi, K., Watkins, A. B., Barnston, A. G., Becker, E. J., Di Liberto, T. E., … Wittenberg, A. T. (2017). Observing and predicting the 2015/16 El Niño. *Bulletin of the American Meteorological Society*, *98*, 1363–1382. https://doi.org/10.1175/BAMS-D-16-0009.1

LA RED. (1992). DesInventar Project. Retrieved from http://www.desenredando.org/

Lagos, P., Silva, Y., Nickl, E., & Mosquera, K. (2008). El Niño-related precipitation variability in Perú. *Advances in Geosciences*, *14*, 231–237. https://doi.org/10.5194/adgeo-14-231-2008

Lavado Casimiro, W., Ronchail, J., Labat, D., Espinoza, J., & Guyot, J. (2012). Basin-scale analysis of rainfall and runoff in Peru (1969–2004): Pacific, Titicaca and Amazonas drainages. *Hydrological Sciences Journal*, *57*(4), 625–642. https://doi.org/10.1080/02626667.2012.672985

Lavado-Casimiro, W., & Espinoza, J. (2014). Impactos de El Niño y La Niña en las lluvias del Perú (1965–2007). *Revista Brasileira de Meteorología*, *29*, 171–182.

Lavado-Casimiro, W., Labat, D., Guyot, J. L., Ronchail, J., & Ordoñez, J. J. (2009). Validation of rainfall using the TRMM for two Peruvian Amazon basins and its inclusion in monthly water balance models. *Revista Peruana Geo-Atmosférica*, *1*, 11–19.

Lavado-Casimiro, W. S., Felipe, O., Silvestre, E., & Bourrel, L. (2013). ENSO impact on hydrology in Peru. *Advances in Geosciences*, *33*, 33–39.

Lenters, J. D., & Cook, K. H. (1995). Simulation and diagnosis of the regional summertime precipitation climatology of South America. *Journal of Climate*, *8*, 2988–3005.

Lenters, J. D., & Cook, K. H. (1997). On the origin of the Bolivian High and related circulation features of the South American climate. *Journal of the Atmospheric Sciences*, *54*, 656–677.

Lenters, J. D., & Cook, K. H. (1999). Summertime precipitation variability over South America: Role of the large-scale circulation. *Monthly Weather Review*, *127*, 409–431.

Liebmann, B., Kiladis, G., Marengo, J., Ambrizzi, T., & Gilck, J. D. (1999). Submonthly convective variability over South America and the South Atlantic convergence zone. *Journal of Climate*, *11*, 2898–2909.

Liu, Z., Lu, Z., Wen, X., Otto-Bliesner, B. L., Timmermann, A., & Cobb, K. M. (2014). Evolution and forcing mechanisms of El Niño over the past 21,000 years. *Nature*, *515*, 550–553.

Lorenz, E. N. (1965). *Empirical orthogonal functions and statistical weather prediction.* Statistical forecasting project (Scientific Report No. 1, 49 p.). Cambridge, MA: Department of Meteorology, Massachusetts Institute of Technology.

Lynch, A., Uotila, P., & Cassano, J. J. (2006). Changes in synoptic weather patterns in the polar regions in the twentieth and twenty-first centuries, part 2: Antarctic. *International Journal of Climatology*, *26*, 1181–1199.

Madden, R., & Julian, P. (1994). A review of the intraseasonal oscillation in the Tropics. *Monthly Weather Review*, *122*, 814–837.

Magilligan, F. J., & Goldstein, P. S. (2001). El Niño floods and culture change: A late Holocene flood history for the Rio Moquegua, southern Peru. *Geology*, *29*, 431–434.

Manz, B., Buytaert, W., Zulkafli, Z., Lavado, W., Willems, B., Robles, L. A., & Rodríguez-Sánchez, J. P. (2016). High-resolution satellite-gauge merged precipitation climatologies of the tropical Andes. *Journal of Geophysical Research: Atmospheres*, *121*, 1190–1207. https://doi.org/10.1002/2015JD023788

Marengo, J., Alves, L., Soares, W., Rodriguez, D., Camargo, H., & Riveros MPabló, A. (2013). Two contrasting severe seasonal extremes in tropical South America in 2012: Flood in Amazonia and drought in northeast Brazil. *Journal of Climate*, *26*(22), 9137–9154. https://doi.org/10.1175/jcli-d-12-00642.1

Marengo, J., Liebmann, B., Grimm, A. M., Misra, V., Silva Dias, P. L., Cavalcanti, I. F. A., … Alves, L. M. (2012). Recent developments on the South American monsoon system. *International Journal of Climatology*, *32*, 1–21.

Marengo, J., Tomasella, J., Soares, W., Alves, L., & Nobre, C. (2012). Extreme climatic events in the Amazon basin. *Theoretical and Applied Climatology*, *107*(1–2), 73–85. https://doi.org/10.1007/s00704-011-0465-1

Marengo, J., Tomasella, J., & Uvo, C. (1998). Trends in streamflow and rainfall in tropical South America: Amazonia, eastern Brazil, and northwestern Peru. *Journal of Geophysical Research: Atmospheres*, *103*(D2), 1775–1783. https://doi.org/10.1029/97jd02551

Marengo, J. A. (1992). Interannual variability of surface climate in the Amazon basin. *International Journal of Climatology*, *12*, 853–863.

Marengo, J. A., & Espinoza, J. (2016). Extreme seasonal droughts and floods in Amazonia: Causes, trends and impacts. *International Journal of Climatology*, *36*(3), 1033–1050. https://doi.org/10.1002/joc.4420

Marengo, J. A., Espinoza, J. C., Alvez, L. M., Ronchail, J., & Baez, J. (2017). Regional climates: Central South America. *Bulletin of the American Meteorological Society*, *98*(8), S187–S190.

Margirier, A., Audin, L., Carcaillet, J., Schwartz, S., & Benavente, C. (2015). Tectonic and climatic controls on the Chuquibamba landslide (western Andes, southern Peru). *Earth Surface Dynamics*, *3*, 281–289. https://doi.org/10.5194/esurf-3-281-2015

McEntire, D. A., & Fuller, C. (2002). The need for a holistic theoretical approach: An examination from El Niño disasters in Peru. *Disaster Prevention and Management*, *11*(2), 128–140.

McPhaden, M. J. (1999). Genesis and evolution of the 1997–98 El Niño. *Science*, *283*, 950–954.

MeteoLab. (2014). MLToolbox [online tutorial]. Retrieved from https://meteo.unican.es/trac/MLToolbox/wiki

Michelangeli, P. A., Vautard, R., & Legras, B. (1995). Weather regimes: Recurrence and quasi-stationarity. *Journal of the Atmospheric Sciences*, *52*, 1237–1256.

Morata, A., Martin, M. L., Luna, M. Y., & Valero, F. (2006). Self-similarity patterns of precipitation in the Iberian Peninsula. *Theoretical and Applied Climatology*, *85*, 41–59.

Morera, S. B., Condom, T., Crave, A., Steer, P., & Guyot, J. L. (2017). The impact of extreme El Niño events on modern sediment transport along the western Peruvian Andes (1968–2012). *Scientific Reports*, *7*(1), 11947. https://doi.org/10.1038/s41598-017-12220-x

Moy, C., Seltzer, G. O., Rodbell, D. T., & Anderson, D. M. (2002). Variability of El Niño/Southern Oscillation activity at millennial timescales during the Holocene epoch. *Nature*, *420*, 162–166.

Muza, M. N., Carvalho, L. M. V., Jones, C., & Liebmann, B. (2009). Intraseasonal and interannual variability of extreme dry and wet events over southeastern South America and the subtropical Atlantic during austral summer. *Journal of Climate*, *22*, 1682–1699.

National Center for Atmospheric Research. (2014). *Outgoing longwave radiation (OLR): AVHRR.* The climate data guide. Boulder, CO: Author. Retrieved from https://climatedataguide.ucar.edu/climate-data/outgoing-longwave-radiation-olr-avhrr

Neukom, R., Rohrer, M., Calanca, P., Salzmann, N., Huggel, C., Acuña, D., … Morales, M. (2015). Facing unprecedented drying of the central Andes? Precipitation variability over the period AD 1000–2100. *Environmental Research Letters*, *10*(8), 084017. https://doi.org/10.1088/1748-9326/10/8/084017

Nickl, E. (2007). *Teleconnections and climate in the Peruvian Andes.* (Unpublished master's thesis). Department of Geography, University of Delaware, Newark, DE.

Paccini, L., Espinoza, J. C., Ronchail, J., & Segura, H. (2018). Intra-seasonal rainfall variability in the Amazon basin related to large-scale circulation patterns: a focus on western Amazon–Andes transition region. *International Journal of Climatology*, *38*, 2386–2399. https://doi.org/10.1002/joc.5341

Peixoto, J. P., & Oort, A. H. (1992). *Physics of climate*. New York, NY: American Institute of Physics.

Power, S., Casey, T., Folland, C., Colman, A., & Mehta, V. (1999). Interdecadal modulation of the impact of ENSO on Australia. *Climate Dynamics*, *15*, 234–319.

Power, S., Delage, F., Chung, C., Kociuba, G., & Keay, K. (2013). Robust twenty-first-century projections of El Niño and related precipitation variability. *Nature*, *502*, 541–545.

Preisendorfer, R., & Mobley, C. D. (1988). *Principal component analysis in meteorology and oceanography Developments in atmospheric science* (Vol. *17*). Amsterdam, Netherlands: Elsevier.

Rau, P., Bourrel, L., Labat, D., Melo, P., Dewitte, B., Frappart, F., … Felipe, O. (2017). Regionalization of rainfall over the Peruvian Pacific slope and coast. *International Journal of Climatology*, *37*, 143–158. https://doi.org/10.1002/joc.4693

Rein, B., Lückge, A., Reinhardt, L., Sirocko, F., Wolf, A., & Dullo, W. C. (2005). El Niño variability off Peru during the last 20,000 years. *Paleoceanography*, *20*, PA4003. https://doi.org/10.1029/2004PA001099

Reusch, D. B., Alley, R. B., & Hewitson, B. C. (2005). Relative performance of self-organizing maps and principal component analysis in pattern extraction from synthetic climatological data. *Polar Geography*, *29*, 227–251.

Reusch, D. B., Alley, R. B., & Hewitson, B. C. (2007). North Atlantic climate variability from a self-organizing map perspective. *Journal of Geophysical Research*, *112*, D02104. https://doi.org/10.1029/2006JD007460

Reusch, D. B., Hewitson, B. C., & Alley, R. B. (2005). Towards ice core-based synoptic reconstructions of West Antarctic climate with artificial neural networks. *International Journal of Climatology*, *25*, 581–610.

Richey, J. E., Nobre, C., & Deser, C. (1989). Amazon river discharge and climate variability: 1903–1985. *Science*, *246*, 101–104.

Richman, M. B. (1986). Rotation of principal components. *Journal of Climatology*, *6*, 293–335.

Rocha, A. (2007). El meganiño 1982-83, "La madre de todos los niños" Conferencia dictada en el II Congreso Internacional "Obras de Saneamiento, Hidráulica, Hidrología y Medio Ambiente" HIDRO 2007- ICG. Lima, Junio 2007.

Ropelewski, C. F., & Halpert, M. S. (2007). Precipitation patterns associated with the high index phase of the Southern Oscillation. *Journal of Climate*, *2*, 268–284.

Schuenemann, K. C., Cassano, J. J., & Finnis, J. (2009). Synoptic forcing of precipitation over Greenland: Climatology for 1961–99. *Journal of Hydrometeorology*, *10*, 60–78.

Seefeldt, M. W., & Cassano, J. J. (2008). An analysis of low-level jets in the Greater Ross ice shelf region based on numerical simulations. *Monthly Weather Review*, *136*, 4188–4205.

Segura, H., Espinoza, J., Junquas, C., & Takahashi, K. (2016). Evidencing decadal and interdecadal hydroclimatic variability over the central Andes. *Environmental Research Letters*, *11*(9), 094016. https://doi.org/10.1088/1748-9326/11/9/094016

Silva Dias, P. L., Schubert, W. H., & De Maria, M. (1983). Large scale response of the tropical atmosphere to transient convection. *Journal of the Atmospheric Sciences*, *40*, 2689–2707.

Skific, N., Francis, J. A., & Cassano, J. J. (2009a). Attribution of projected changes in atmospheric moisture transport in the Arctic: A self-organizing map perspective. *Journal of Climate*, *22*, 4135–4153.

Skific, N., Francis, J. A., & Cassano, J. J. (2009b). Attribution of seasonal and regional changes in Arctic moisture convergence. *Journal of Climate*, *22*, 5115–5134.

Smith, T. M., Reynolds, R. W., Livezey, R. E., & Stokes, D. C. (1996). Reconstruction of historical sea surface temperatures using empirical orthogonal functions. *Journal of Climate*, *9*(6), 1403–1420.

Su, J., Li, T., & Zhang, R. (2014). The initiation and developing mechanisms of Central Pacific El Niño. *Journal of Climate*, *27*, 4473–4485. https://doi.org/10.1175/JCLI-D-13-00640.1

Sulca, J., Takahashi, K., Espinoza, J., Vuille, M., & Lavado-Casimiro, W. (2017). Impacts of different ENSO flavors and tropical Pacific convection variability (ITCZ, SPCZ) on austral summer rainfall in South America, with a focus on Peru. *International Journal of Climatology*, *38*, 420–435. https://doi.org/10.1002/joc.5185

Sulca, J., Vuille, M., Silva, Y., & Takahashi, K. (2016). Teleconnections between the Peruvian central Andes and northeast Brazil during extreme rainfall events in austral summer. *Journal of Hydrometeorology*, *17*, 499–515.

Takahashi, K. (2004). The atmospheric circulation associated with extreme rainfall events in Piura, Peru, during the 1997–1998 and 2002 El Niño events. *Annales Geophysicae*, *22*(11), 3917–3926. https://doi.org/10.5194/angeo-22-3917-2004

Takahashi, K., & Martínez, A. G. (2017). The very strong coastal El Niño in 1925 in the far-eastern Pacific. *Climate Dynamics*. https://doi.org/10.1007/s00382-017-3702-1

Takahashi, K., Montecinos, A., Goubanova, K., & Dewitte, B. (2011). ENSO regimes: Reinterpreting the canonical and Modoki El Niño. *Geophysical Research Letters*, *38*, L10704. https://doi.org/10.1029/2011GL047364

Uotila, P., Lynch, A. H., Cassano, J. J., & Cullather, R. I. (2007). Changes in Antarctic net precipitation in the 21st century based on Intergovernmental Panel on Climate Change (IPCC) model scenarios. *Journal of Geophysical Research*, *112*, D10107. https://doi.org/10.1029/2006JD007482

Uppala, S. M., Kallberg, P. W., Simmons, A. J., Andrae, U., Da Costa Bechtold, V., Fiorino, M., … Woollen, J. (2005). The ERA-40 re-analysis. *Quarterly Journal of the Royal Meteorological Society*, *131*, 2961–3012.

Van den Dool, H. M., Saha, S., & Johansson, Å. (2000). Empirical orthogonal teleconnections. *Journal of Climate*, *13*, 1421–1435.

Vargas, R. D., Thouret, J. C., Delaite, G., Van Westen, C. J., Sheridan, M. F., Siebe, C., … Stinton, A. (2010). Mapping and assessing volcanic and flood hazards and risks, with emphasis on lahars, in Arequipa, Peru. In G. Groppelli & L. Viereck-Goette (Eds.), *Stratigraphy and geology of volcanic areas Geological Society of America special paper* (Vol. *464*, pp. 265–280). https://doi.org/10.1130/2010.2464(13)

Vera, C., Higgins, W., Amador, J., Ambrizzi, T., Garreaud, R., Gochis, D., … Zhang, C. (2006). Towards a unified view of the American monsoon system. *Journal of Climate*, *19*, 4977–5000.

Villacorta, S., De Torres, D., Pérez-Puig, C., Llorente, M., & Ayala, L. (2015). Estudio preliminar de la evolución geomorfológica del abanico aluvial de Lima (Perú) e implicancias en el análisis de amenazas asociadas al cambio climático. *Series Correlación Geológica*, *31*(2), 173–182.

Villacorta, S., Fidel, L., & Zavala, B. (2012). Mapa de susceptibilidad por movimientos en masa del Perú. *Revista de la Asociación Geológica Argentina*, *69*(3), 393–399.

Von Storch, H., & Zwiers, F. W. (1999). *Statistical analysis in climate research*. Cambridge, England: Cambridge University Press.

Vuille, M. (1999). Atmospheric circulation over the Bolivian Altiplano during dry and wet periods and extreme phases of the Southern Oscillation. *International Journal of Climatology*, *19*, 1579–1600.

Vuille, M., Bradley, R., & Keimig, F. (2000). Interannual climate variability in the central Andes and its relation to tropical Pacific and Atlantic forcing. *Journal of Geophysical Research: Atmospheres*, *105*(D10), 12447–12460. https://doi.org/10.1029/2000jd900134

Vuille, M., Bradley, R., Werner, M., & Keimig, F. (2003). 20th century climate change in the tropical Andes: Observations and model results. *Climatic Change*, *59*, 75–99.

Vuille, M., & Keimig, F. (2004). Interannual variability of summertime convective cloudiness and precipitation in the central Andes derived from ISCCP-B3 data. *Journal of Climate*, *17*, 3334–3348.

Walsh, J. E. (1978). Temporal and spatial scales of Arctic circulation. *Monthly Weather Review*, *106*(11), 1532–1544.

Waylen, P. R., & Caviedes, C. N. (1986). El Niño and annual floods on the north Peruvian littoral. *Journal of Hydrology*, *89*, 141–156.

Wise, E., & Dannenberg, M. (2014). Persistence of pressure patterns over North America and the North Pacific since AD 1500. *Nature Communications*, *5*, 4912. https://doi.org/10.1038/ncomms5912

Wisner, B., Blaikie, P. M., Cannon, T., & Davis, I. (2004). *At risk: Natural hazards, people's vulnerability and disasters*. London, England: Routledge.

Wittenberg, A. (2009). Are historical records sufficient to constrain ENSO simulations. *Geophysical Research Letters*, *36*, L12702. https://doi.org/10.1029/2009GL038710

World Meteorological Organization. (2014). *El Niño/Southern Oscillation* (WMO No. 1145). Geneva, Switzerland: Author.

Yoon, J., & Zeng, N. (2010). An Atlantic influence on Amazon rainfall. *Climate Dynamics*, *34*(2–3), 249–264. https://doi.org/10.1007/s00382-009-0551-6

Young, K. R., & León, B. (2009). Natural hazards in Peru: Causation and vulnerability. *Developments in Earth Surface Processes*, *13*, 165–180. https://doi.org/10.1016/S0928-2025(08)10009-8

Yu, J. Y., Kao, H. Y., & Lee, T. (2010). Subtropics-related interannual sea surface temperature variability in the central equatorial Pacific. *Journal of Climate*, *23*, 2869–2884. https://doi.org/10.1175/2010JCLI3171.1

Zavala, B. L., & Núñez, S. (1999). *Estudio geológico geotécnico de la región suroccidental del Perú Boletín, Serie C: Geodinámica e Ingeniería Geológica* (Vol. *22*, 1st ed.). Lima, Peru: INGEMMET.

Zavala, B. L., Rosado, M., & León, S. L. (2012). Susceptibilidad a los movimientos en masa en la región Cajamarca, norte de Perú y el deslizamiento de Rodeopampa del 22 de Febrero del 2010. *Revista de la Asociación Geológica Argentina*, *69*(3), 407–417.

Zhang, R., Wang, Y., Liu, W., Ahu, W., & Wang, J. (2006). Cloud classification based on self-organizing feature map and probabilistic neural network. In *Proceedings of the 6th world congress on intelligent control and automation* (pp. 41–45). Dalian, China: IEEE.

Zhou, J., & Lau, K. M. (1998). Does a monsoon climate exist over South America? *Journal of Climate*, *11*, 1020–1040.

SUPPORTING INFORMATION

Additional Supporting Information may be found online in the supporting information tab for this article.

How to cite this article: Rodríguez-Morata C, Ballesteros-Canovas JA, Rohrer M, Espinoza JC, Beniston M, Stoffel M. Linking atmospheric circulation patterns with hydro-geomorphic disasters in Peru. *Int J Climatol*. 2018;1–17. https://doi.org/10.1002/joc.5507